symmetry

IMPACT FACTOR 2.2

CITESCORE 5.4

Review

Overview of $B \to K^{(*)}\ell\ell$ Theoretical Calculations and Uncertainties

Farvah Mahmoudi and Yann Monceaux

Special Issue

Symmetries and Anomalies in Flavour Physics

Edited by

Dr. Stefania Ricciardi, Dr. Thomas Blake and Dr. Farvah Nazila Mahmoudi

MDPI

https://doi.org/10.3390/sym16081006

symmetry

MDPI

Review

Overview of $B \to K^{(*)}\ell\ell$ Theoretical Calculations and Uncertainties

Farvah Mahmoudi [1,2,3,*] and Yann Monceaux [1,*]

[1] Institut de Physique des 2 Infinis de Lyon, UMR 5822, Université Claude Bernard Lyon 1, CNRS/IN2P3, 69622 Villeurbanne, France
[2] Theoretical Physics Department, CERN, CH-1211 Geneva, Switzerland
[3] Institut Universitaire de France (IUF), 75005 Paris, France
* Correspondence: nazila@cern.ch (F.M.); y.monceaux@ip2i.in2p3.fr (Y.M.)

Abstract: The search for New Physics (NP) beyond the Standard Model (SM) has been a central focus of particle physics, including in the context of B-meson decays involving $b \to s\ell\ell$ transitions. These transitions, mediated by flavour-changing neutral currents, are highly sensitive to small NP effects due to their suppression in the SM. While direct searches at colliders have not yet led to NP discoveries, indirect probes through semi-leptonic decays have revealed anomalies in observables such as the branching fraction $\mathcal{B}(B \to K\mu\mu)$ and the angular observable $P_5'(B \to K^*\mu\mu)$. In order to assess the observed tensions, it is essential to ensure an accurate SM prediction. In this review, we examine the theoretical basis of the $B \to K^{(*)}\ell\ell$ decays, addressing in particular key uncertainties arising from local and non-local form factors. We also discuss the impact of QED corrections to the Wilson coefficients, as well as the effect of CKM matrix elements on the predictions and the tension with the experimental measurements. We discuss the most recent results, highlighting ongoing efforts to refine predictions and to constrain potential signs of NP in these critical decay processes.

Keywords: B physics; semi-leptonic decays; form factors; charm loops

Citation: Mahmoudi, F.; Monceaux, Y. Overview of $B \to K^{(*)}\ell\ell$ Theoretical Calculations and Uncertainties. *Symmetry* **2024**, *16*, 1006. https://doi.org/10.3390/sym16081006

Academic Editor: Francesco Renga

Received: 10 July 2024
Revised: 31 July 2024
Accepted: 2 August 2024
Published: 7 August 2024

1. Introduction

The discovery of the Higgs boson at the LHC in 2012 [1,2] marked a significant milestone in validating the Standard Model (SM) of particle physics. However, the SM remains an incomplete theory; thus, the search for New Physics (NP) signals including NP particles has been ongoing at colliders. Although direct searches have not yet led to discoveries, several hints of potential NP have been observed via indirect searches. Semi-leptonic B-meson decays via $b \to s\ell^+\ell^-$ transitions have been prime candidates for probing NP indirectly. These transitions mediated by flavour-changing neutral currents are forbidden at the tree level in the SM and are further suppressed by elements of the Cabibbo–Kobayashi–Maskawa (CKM) matrix, making them particularly sensitive to small NP effects. Numerous deviations from SM predictions, often referred to as anomalies, have been observed in these decays. An intriguing tension was found in the lepton flavour universality ratios $R_{K^{(*)}}$ of $B \to K^{(*)}\ell^+\ell^-$ where the ratio is between a final state with a muon pair and an electron pair. However, recent results from LHCb now indicate an SM-like behaviour with no significant deviations observed [3]. Still, deviations remain in other observables such as the branching fraction $\mathcal{B}(B \to K\mu^+\mu^-)$ [4–7], and the angular observable $P_5'(B \to K^*\mu^+\mu^-)$ [8–13] at low q^2 where q^2 denotes the invariant squared mass of the dilepton in the final state. Recent measurements by CMS [7,13] confirm previous observations by LHCb [6,8,9], indicating a persistent tension with the theoretical predictions.

However, branching fractions and, to a lesser degree, the optimised angular observables P_i, are more challenging to predict than the $R_{K^{(*)}}$ ratios and suffer from larger uncertainties.

In this review, we address the calculation of $B \to K^{(*)}\ell\ell$ observables. In Section 2, we introduce the notations and key observables. We then turn to the current state of local and non-local form factors in Sections 3 and 4, which constitute the primary sources of uncertainty in these calculations. In Section 5, we address the impact of QED corrections to Wilson coefficients as well as the effect of CKM matrix elements, which become increasingly significant as precision increases. Section 6 presents a quantitative assessment of the implications of different theoretical predictions. Finally, Section 7 provides our conclusions.

2. Theoretical Framework

$B \to K^{(*)}\ell^+\ell^-$ decays are well described in the Weak Effective Theory. In this formalism, the transition $b \to s\ell^+\ell^-$ is described by an effective Hamiltonian, where degrees of freedom above the electroweak scale have been integrated out [14–16]:

$$\mathcal{H}_{\text{eff}} = -\frac{4G_F}{\sqrt{2}}\left\{\lambda_t\left(\sum_{i=1}^{i=2} C_i\mathcal{O}_i^c + \sum_{i=3}^{i=6} C_i\mathcal{O}_i + \sum_{i=7,8,9,10}(C_i\mathcal{O}_i + C_i'\mathcal{O}_i')\right) + \lambda_u\left(\sum_{i=1}^{i=2} C_i(\mathcal{O}_i^c - \mathcal{O}_i^u)\right)\right\} + \text{h.c.} \tag{1}$$

The CKM factor λ_j denotes $\lambda_j = V_{jb}V_{js}^*$ and G_F is the Fermi coupling constant. The local operators $\mathcal{O}_i$ and their associated Wilson coefficients C_i are given in the standard basis introduced in [17] by

$$\begin{aligned}
\mathcal{O}_1^q &= (\bar{s}_L\gamma_\mu T^a q_L)(\bar{q}_L\gamma^\mu T^a b_L), & \mathcal{O}_2^q &= (\bar{s}_L\gamma_\mu q_L)(\bar{q}_L\gamma^\mu b_L),\\
\mathcal{O}_3 &= (\bar{s}_L\gamma_\mu b_L)\sum_{q'}(\bar{q}'\gamma^\mu q'), & \mathcal{O}_4 &= (\bar{s}_L\gamma_\mu T^a b_L)\sum_{q'}(\bar{q}'\gamma^\mu T^a q'),\\
\mathcal{O}_5 &= (\bar{s}_L\gamma_{\mu_1}\gamma_{\mu_2}\gamma_{\mu_3} b_L)\sum_{q'}(\bar{q}'\gamma^{\mu_1}\gamma^{\mu_2}\gamma^{\mu_3} q'), & \mathcal{O}_6 &= (\bar{s}_L\gamma_{\mu_1}\gamma_{\mu_2}\gamma_{\mu_3} T^a b_L)\sum_{q'}(\bar{q}'\gamma^{\mu_1}\gamma^{\mu_2}\gamma^{\mu_3} T^a q'),\\
\mathcal{O}_7 &= \frac{e}{16\pi^2} m_b(\bar{s}\sigma^{\mu\nu} P_R b)F_{\mu\nu}, & \mathcal{O}_8 &= \frac{g_s}{16\pi^2} m_b(\bar{s}\sigma^{\mu\nu} P_R T^a b)G^a_{\mu\nu},\\
\mathcal{O}_9 &= \frac{e^2}{16\pi^2}(\bar{s}\gamma_\mu P_L b)(\bar{l}\gamma^\mu l), & \mathcal{O}_{10} &= \frac{e^2}{16\pi^2}(\bar{s}\gamma_\mu P_L b)(\bar{l}\gamma^\mu\gamma_5 l),
\end{aligned} \tag{2}$$

where g_s is the strong coupling constant; the quark flavour $q = u, c$; the lepton flavour $l = e, \mu, \tau$; and m_b is the running b-quark mass in the $\overline{\text{MS}}$ scheme. We use the conventions $P_{L,R} = (1 \mp \gamma_5)/2$ and $\sigma_{\mu\nu} = \frac{i}{2}[\gamma_\mu, \gamma_\nu]$. The primed local operators $\mathcal{O}_i$ are obtained by performing the exchange $P_L \leftrightarrow P_R$.

The term proportional to λ_u in the definition (1) is often neglected as it is strongly CKM-suppressed with respect to the term proportional to λ_t. However, it can be relevant for observables that are specifically sensitive to complex phases of decay amplitudes. We discard it in the following.

The decay amplitude reads as follows:

$$A(B \to K^{(*)}\ell^+\ell^-) = -\langle K^{(*)}(k)\ell^+\ell^-|\,\mathcal{H}_{\text{eff}}\,|B(p_B = k+q)\rangle\,, \tag{3}$$

which leads to the expression [18–20]

$$\begin{aligned}
A(B \to K^{(*)}\ell^+\ell^-) \equiv \frac{G_F\,\alpha\,V_{tb}V_{ts}^*}{\sqrt{2}\pi}\Big\{&(C_9\,L_V^\mu + C_{10}\,L_A^\mu)\,\mathcal{F}_\mu^{B\to K^{(*)}}\\
&- \frac{L_V^\mu}{q^2}\left[2im_b C_7\,\mathcal{F}_{T,\mu}^{B\to K^{(*)}} + 16\pi^2\mathcal{H}_\mu^{B\to K^{(*)}}\right]\Big\}.
\end{aligned} \tag{4}$$

Here, α denotes the electromagnetic coupling constant, $L^{\mu}_{V,A}$ are leptonic currents, and $\mathcal{F}_{(T),\mu}$ and $\mathcal{H}_{\mu}$ are, respectively, local and non-local hadronic matrix elements. They are given by

$$L^{\mu}_{V} \equiv \bar{u}_{\ell}(q_1)\gamma^{\mu}v_{\ell}(q_2)\,, \tag{5}$$

$$L^{\mu}_{A} \equiv \bar{u}_{\ell}(q_1)\gamma^{\mu}\gamma_5 v_{\ell}(q_2)\,, \tag{6}$$

$$\mathcal{F}^{B\to K^{(*)}}_{\mu} \equiv \langle \bar{K}^{(*)}(k)|\,\bar{s}\gamma_{\mu}P_L b\,|\bar{B}(p_B = k+q)\rangle\,, \tag{7}$$

$$\mathcal{F}^{B\to K^{(*)}}_{T,\mu} \equiv \langle \bar{K}^{(*)}(k)|\,\bar{s}\sigma_{\mu\nu}q^{\nu}P_L b\,|\bar{B}(p_B = k+q)\rangle\,, \tag{8}$$

$$\mathcal{H}^{B\to K^{(*)}}_{\mu} \equiv \sum_{q'}\mathcal{H}^{B\to K^{(*)}}_{q',\mu}\,. \tag{9}$$

In the last term $\mathcal{H}^{B\to K^{(*)}}_{\mu}$, the sum runs over the accessible quark flavours (at the typical scale $\mu_b = m_b$) $q' = u, d, s, c, b$. For a given quark flavour,

$$\mathcal{H}^{B\to K^{(*)}}_{q',\mu}(q,k) \equiv iQ_{q'}\int d^4x e^{iq\cdot x} \times \langle \bar{K}^{(*)}(k)|\,T\Big\{\bar{q}'\gamma_{\mu}q'(x),\Big(\sum_{i=1}^{i=2}C_i\mathcal{O}^c_i + \sum_{i=3}^{i=6}C_i\mathcal{O}_i + C_8\mathcal{O}_8\Big)(0)\Big\}\,|\bar{B}(k+q)\rangle\,, \tag{10}$$

where $Q_{q'}$ denotes the electric charge of the quark q'. The local operators $\mathcal{O}^c_1$ and $\mathcal{O}^c_2$ have been singled out in (1) and (10), as they numerically contribute more than the other hadronic operators $\mathcal{O}_{3-6}$.

The expression (4) is obtained at leading order in QED. The QED effects have been discussed in [21–23] where the $\mathcal{O}(\alpha)$ corrections have been computed. For the partial width, the reduction is estimated to be up to 10% at high q^2 for muons in the final state, while it is even larger when considering electrons in the final state. Such effects are accounted for on the experimental side with software like `PHOTOS` [24] before comparison with the theoretical predictions.

In the following, we describe briefly the calculation of $B \to K\ell^+\ell^-$ and $B \to K^*\ell^+\ell^-$ observables. For detailed descriptions, we refer the reader to the `SuperIso` manual [25].

2.1. $B \to K\ell^+\ell^-$

The full differential distribution of the $B \to K\ell^+\ell^-$ decay can be expressed in the SM as [26,27]

$$\frac{d^2\Gamma(\bar{B}\to\bar{K}\ell^+\ell^-)}{dq^2 d\cos\theta} = a_{\ell}(q^2) + c_{\ell}(q^2)\cos\theta^2, \tag{11}$$

where θ is defined as the angle between the directions of the lepton ℓ^- and the $\bar{B}$-meson in the rest frame of the lepton pair. The boundaries of the phase space are given by

$$4m^2_{\ell} \le q^2 \le (m_B - m_K)^2, \qquad -1 \le \cos\theta \le 1. \tag{12}$$

The functions a_{ℓ} and c_{ℓ} in Equation (11) are defined in the SM as follows:

$$a_{\ell}(q^2) = \mathcal{C}(q^2)\Big[q^2|F_P(q^2)|^2 + \frac{\lambda(m_B^2, m_K^2, q^2)}{4}\Big(|F_A(q^2)|^2 + |F_V(q^2)|^2\Big) + 4m^2_{\ell}m^2_B|F_A(q^2)|^2 + 2m_{\ell}\Big(m_B^2 - m_K^2 + q^2\Big)\mathrm{Re}\Big(F_P(q^2)F_A^*(q^2)\Big)\Big], \tag{13}$$

$$c_{\ell}(q^2) = \mathcal{C}(q^2)\Big[-\frac{\lambda(m_B^2, m_K^2, q^2)}{4}\beta^2_{\ell}(q^2)\Big(|F_A(q^2)|^2 + |F_V(q^2)|^2\Big)\Big], \tag{14}$$

with the prefactor

$$\mathcal{C}(q^2) \equiv \frac{G_F^2 \alpha^2 |V_{tb} V_{ts}^*|^2}{512\pi^5 m_B^3} \beta_\ell(q^2) \sqrt{\lambda(m_B^2, m_K^2, q^2)}, \tag{15}$$

where $\beta_\ell(q^2) \equiv \sqrt{1 - 4\frac{m_\ell^2}{q^2}}$ for $\ell = e, \mu, \tau$, and λ is the Källén function:

$$\lambda(x, y, z) = x^2 + y^2 + z^2 - 2(xy + yz + xz). \tag{16}$$

In the above equations, F_V, F_A, and F_P can be written in the SM as [26]

$$F_V(q^2) = (C_9 + C_9^{'}) f_+(q^2) + \frac{2m_b}{m_B + m_K}(C_7^{\text{eff}} + C_7^{'}) f_T(q^2) + \delta F_V, \tag{17}$$

$$F_A(q^2) = (C_{10} + C_{10}^{'}) f_+(q^2), \tag{18}$$

$$F_P(q^2) = -m_l(C_{10} + C_{10}^{'}) \Big[f_+(q^2) - \frac{m_B^2 - m_K^2}{q^2}(f_0(q^2) - f_+(q^2)) \Big], \tag{19}$$

where C_7^{eff} is defined in Equation (47). The local form factors f_+, f_0, and f_T are defined in Appendix A and their calculations are discussed in Section 3. The term δF_V corresponds to non-local contributions and is addressed in more detail in Section 4. Appendix C introduces the alternative form factor basis proposed in [20], establishing the correspondence between their transversity amplitudes and the F_i functions, as well as the correspondence of the non-local term.

Observables

It is customary to introduce the q^2-integrated coefficients [26,27]

$$A_\ell = \int_{q^2_{\text{min}}}^{q^2_{\text{max}}} dq^2 a_\ell(q^2), \qquad C_\ell = \int_{q^2_{\text{min}}}^{q^2_{\text{max}}} dq^2 c_\ell(q^2), \tag{20}$$

to express the observables. The decay rate can then be written as

$$\Gamma(B \to K\ell^+\ell^-) = 2\Big(A_\ell + \frac{1}{3}C_\ell\Big), \tag{21}$$

and the flat-term is

$$F_H^\ell = \frac{2}{\Gamma_\ell}(A_\ell + C_\ell). \tag{22}$$

In the SM, the forward–backward asymmetry is null and the flat term is proportional to m_ℓ. However, they can receive sizeable NP contributions, which make them relevant observables.

2.2. $B \to K^*\ell^+\ell^-$

For $\bar{B} \to \bar{K}^*\ell^+\ell^-$, the process that is measured is $\bar{B} \to \bar{K}^*(\to K\pi)\ell^+\ell^-$. The subsequent decay $K^* \to K\pi$ can be described with the effective Hamiltonian [28]:

$$\mathcal{H}_{\text{eff}} = g_{K^*K\pi}(p_K - p_\pi) \cdot \varepsilon_{K^*}, \tag{23}$$

where $g_{K^*K\pi}$ is the coupling constant and ε_{K^*} is the polarisation of the K^* meson. It is convenient to consider the K^*-meson on the mass-shell when using a narrow-width approximation [28–30] and to replace the squared K^* propagator by

$$\frac{1}{(p_{K^*}^2 - m_{K^*}^2)^2 + (m_{K^*}\Gamma_{K^*})^2} \xrightarrow{\Gamma_{K^*} \ll m_{K^*}} \frac{\pi}{m_{K^*}\Gamma_{K^*}} \delta(p_{K^*}^2 - m_{K^*}^2). \tag{24}$$

Since the width of the K^* meson can be written as

$$\Gamma_{K^*} = \frac{g^2_{K^*K\pi}}{48\pi} m_{K^*} \beta^3, \tag{25}$$

where β is related to the Källén function as

$$\beta = \frac{1}{m^2_{K^*}} \lambda(m^2_{K^*}, m^2_K, m^2_\pi)^{1/2}, \tag{26}$$

the final result in this narrow-width limit is independent of the coupling $g_{K^*K\pi}$ which cancels out. The impact of the finite width of the K^*-meson is addressed in Section 3.

In the narrow-width approximation, summing over the lepton spins, the full differential distribution can be written as [28,29,31–33]

$$\frac{d^4\Gamma}{dq^2 d\cos\theta_\ell d\cos\theta_{K^*} d\phi} = \frac{9}{32\pi} J(q^2, \theta_\ell, \theta_{K^*}, \phi). \tag{27}$$

We work in the convention where θ_ℓ is defined as the angle between the directions of the lepton ℓ^- and the $\bar{B}$-meson in the rest frame of the lepton pair, θ_{K^*} is the angle between the directions of the K-meson and the $\bar{B}$-meson in the $K\pi$ rest frame, and ϕ is the angle between the normals of the plane of $K\pi$ and the plane of the lepton pair. In [29,31], the convention for θ_ℓ is slightly different. More details about the angles and conventions are given in Appendix B.

The boundaries of the phase space are

$$4m^2_\ell \le q^2 \le (m_B - m_{K^*})^2, \quad -1 \le \cos\theta_\ell \le 1, \quad -1 \le \cos\theta_{K^*} \le 1, \quad 0 \le \phi \le 2\pi. \tag{28}$$

The explicit expression of J is

$$\begin{aligned} J(q^2, \theta_k, \theta_l, \phi) =& J^c_1 \cos^2\theta_k + J^s_1 \sin^2\theta_k + (J^c_2 \cos^2\theta_k + J^s_2 \sin^2\theta_k)\cos 2\theta_l + J_3 \sin^2\theta_k \sin^2\theta_l \cos 2\phi \\ &+ J_4 \sin 2\theta_k \sin 2\theta_l \cos\phi + J_5 \sin 2\theta_k \sin\theta_l \cos\phi + J_6 \sin^2\theta_k \cos\theta_l \\ &+ J_7 \sin 2\theta_k \sin\theta_l \sin\phi + J_8 \sin 2\theta_k \sin 2\theta_l \sin\phi + J_9 \sin^2\theta_k \sin^2\theta_l \sin 2\phi. \end{aligned} \tag{29}$$

The angular coefficients J^a_i with $i = 1, \ldots, 9$ and $a = s, c$ can be expressed with the transversity amplitudes $A_0, A_\parallel, A_\perp$:

$$\begin{aligned} J^c_1 &= |A^L_0|^2 + |A^R_0|^2 + \frac{4m^2_l}{q^2}\left(|A_t|^2 + 2\,\mathrm{Re}(A^L_0 A^{L*}_0)\right), & J^c_2 &= -\beta^2_l(|A^L_0|^2 + |A^R_0|^2), \\ J^s_1 &= \frac{2+\beta^2_l}{4}\left(|A^L_\perp|^2 + |A^L_\parallel|^2 + (L \leftrightarrow R)\right) & J^s_2 &= \frac{\beta^2_l}{4}\left(|A^L_\parallel|^2 + |A^L_\perp|^2 + (L \leftrightarrow R)\right), \\ &\quad + \frac{4m^2_l}{q^2}\left(\mathrm{Re}(A^L_\parallel A^{R*}_\parallel) + \mathrm{Re}(A^L_\perp A^{R*}_\perp)\right), & J_3 &= \frac{\beta^2_l}{2}\left(|A^L_\perp|^2 - |A^L_\parallel|^2 + (L \leftrightarrow R)\right), \\ J_4 &= \frac{\beta^2_l}{\sqrt{2}}\left(\mathrm{Re}(A^L_0 A^{L*}_\parallel) + (L \leftrightarrow R)\right), & J_5 &= \sqrt{2}\beta_l\left(\mathrm{Re}(A^L_0 A^{L*}_\perp) - (L \leftrightarrow R)\right), \\ J_6 &= 2\beta_l\left(\mathrm{Re}(A^L_\parallel A^{L*}_\perp) - (L \leftrightarrow R)\right), & J_7 &= \sqrt{2}\beta_l\left(\mathrm{Im}(A^L_0 A^{L*}_\parallel) - (L \leftrightarrow R)\right), \\ J_8 &= \frac{\beta^2_l}{\sqrt{2}}\left(\mathrm{Im}(A^L_0 A^{L*}_\perp) + (L \leftrightarrow R)\right), & J_9 &= \beta^2_l\left(\mathrm{Im}(A^{L*}_\parallel A^L_\perp) + (L \leftrightarrow R)\right), \end{aligned} \tag{30}$$

where, again, $\beta_\ell(q^2) = \sqrt{1 - 4\frac{m^2_\ell}{q^2}}$.

The transversity amplitudes can be written as follows:

$$
\begin{aligned}
A_0^{L,R} &= -\frac{N}{2m_{K^*}\sqrt{q^2}}\Bigg[\Big((C_9 - C_9^{'}) \mp (C_{10} - C_{10}^{'})\Big)[(m_B^2 - m_{K^*}^2 - q^2)(m_B + m_{K^*})A_1 \\
&\quad - \frac{\lambda(m_B^2, m_{K^*}^2, q^2)}{m_B + m_{K^*}}A_2] + 2m_b(C_7^{\text{eff}} - C_7^{'})[(3m_{K^*}^2 + m_B^2 - q^2)T_2 - \frac{\lambda(m_B^2, m_{K^*}^2, q^2)}{m_B^2 - m_{K^*}^2}T_3]\Bigg] + \delta A_0^{L,R}, \\
A_\perp^{L,R} &= N\sqrt{2\lambda(m_B^2, m_{K^*}^2, q^2)}\Bigg[\Big((C_9 + C_9^{'}) \mp (C_{10} + C_{10}^{'})\Big)\frac{V}{m_B + m_{K^*}} + 2m_b\frac{C_7^{\text{eff}} + C_7^{'}}{q^2}T_1\Bigg] + \delta A_\perp^{L,R}, \\
A_\parallel^{L,R} &= -N\sqrt{2}\Bigg[\Big((C_9 - C_9^{'}) \mp (C_{10} - C_{10}^{'})\Big)(m_B + m_{K^*})A_1 + 2m_b\frac{C_7^{\text{eff}} - C_7^{\prime}}{q^2}(m_B^2 - m_{K^*}^2)T_2\Bigg] + \delta A_\parallel^{L,R}, \\
A_t &= 2N(C_{10} - C_{10}^{'})\frac{\sqrt{\lambda(m_B^2, m_{K^*}^2, q^2)}}{\sqrt{q^2}}A_0,
\end{aligned}
\tag{31}
$$

with the prefactor

$$
N = V_{tb}V_{ts}^*\left[\frac{\alpha^2 G_F^2}{3 \times 2^{10}\pi^5 m_B^3}q^2\beta_l\sqrt{\lambda(m_B^2, m_{K^*}^2, q^2)}\right]^{1/2}.
$$

The local form factors $V, A_0, A_1, A_2, T_1, T_2$, and T_3 are defined in Appendix A and their calculations are discussed in Section 3. The terms δA_i correspond to non-local contributions, which are addressed in more detail in Section 4. Appendix C introduces the alternative form factor basis suggested in [20], and establishes the correspondence between their transversity amplitudes and the ones introduced in this section, as well as the correspondence of the non-local terms.

For the CP-conjugated decay $B \to K^*\ell^-\ell^+$, the full differential distribution can be written as [32,34]

$$
\frac{d^4\bar{\Gamma}}{dq^2 d\cos\theta_\ell d\cos\theta_{K^*} d\phi} = \frac{9}{32\pi}\bar{J}(q^2, \theta_\ell, \theta_{K^*}, \phi). \tag{32}
$$

The explicit expression of $\bar{J}(q^2, \theta_\ell, \theta_{K^*}, \phi)$ can be derived from that of $J(q^2, \theta_\ell, \theta_{K^*}, \phi)$ in Equation (29) while performing the following replacements:

$$
J_{1,2,3,4,7}^{(a)} \to \bar{J}_{1,2,3,4,7}^{(a)}, \qquad J_{5,6,8,9} \to -\bar{J}_{5,6,8,9}, \tag{33}
$$

where $\bar{J}_i^{(a)}$ is obtained by conjugating all weak phases in $J_i^{(a)}$.

The relative signs when going from $J_i^{(a)}$ to $\bar{J}_i^{(a)}$ can be understood from transforming the angles as $(\theta_l, \theta_{K^*}, \phi) \to (\pi - \theta_l, \pi - \theta_{K^*}, 2\pi - \phi)$, which is the usual convention.

Observables

We introduce below some of the key observables for the $\bar{B} \to \bar{K}^*\ell^+\ell^-$ decay. The dilepton-invariant mass spectrum is obtained by integrating the full differential distribution over all three angles [32]:

$$
\frac{d\Gamma}{dq^2} = \frac{3}{4}\Big(J_1 - \frac{J_2}{3}\Big), \tag{34}
$$

where, for convenience,

$$
J_{1,2} \equiv 2J_{1,2}^s + J_{1,2}^c. \tag{35}
$$

The normalised forward–backward asymmetry is defined as [35]

$$
\begin{aligned}
A_{FB}(q^2) &\equiv \left[\int_{-1}^{0} - \int_{0}^{1}\right] d\cos\theta_l \frac{d^2\Gamma}{dq^2 d\cos\theta_l} \Big/ \frac{d\Gamma}{dq^2} \\
&= -\frac{3}{8}\frac{2J_6}{d\Gamma/dq^2}.
\end{aligned}
\tag{36}
$$

In [29,32,36–38], the global sign is different in the definition of the forward–backward-asymmetry.

The K^*-meson polarisation fractions F_L and F_T are given by [31,35,36,38]

$$F_L(q^2) = \frac{3J_1^c - J_2^c}{4d\Gamma/dq^2}, \qquad F_T(q^2) = \frac{4J_2^s}{d\Gamma/dq^2}, \tag{37}$$

and the K^*-meson polarisation parameter reads as follows [31]:

$$\alpha_{K^*}(q^2) = 2\frac{F_L}{F_T} - 1. \tag{38}$$

A set of theoretically clean angular observables has been introduced in [31,35], designed to be less sensitive to form factors. Primed angular observables were later introduced in [39]. They are defined in the SM as

$$\begin{aligned}
P_1(q^2) &= \frac{J_3}{2J_2^s}, & P_2(q^2) &= \beta_\ell \frac{J_6}{8J_2^s},\\
P_3(q^2) &= -\frac{J_9}{4J_2^s}, & P_4(q^2) &= \frac{\sqrt{2}J_4}{\sqrt{-J_2^c(2J_2^s - J_3)}},\\
P_5(q^2) &= \frac{\beta_\ell J_5}{\sqrt{-2J_2^c(2J_2^s + J_3)}}, & P_6(q^2) &= -\frac{\beta_\ell J_7}{\sqrt{-2J_2^c(2J_2^s - J_3)}},\\
P_4'(q^2) &= \frac{J_4}{\sqrt{-J_2^c J_2^s}}, & P_5'(q^2) &= \frac{J_5}{2\sqrt{-J_2^c J_2^s}},\\
P_6'(q^2) &= -\frac{J_7}{2\sqrt{-J_2^c J_2^s}}.
\end{aligned} \tag{39}$$

For all of the observables given in this section, one can define the CP-average quantities, which are often the ones measured experimentally.

3. Local Form Factors

Local form factors can be computed in lattice QCD or with QCD sum rules on the light-cone. Lattice QCD determinations, based on first principles, are typically more accurate and reliable but are mostly limited to the low-recoil region (high q^2). Light-Cone Sum Rules (LCSRs) can bridge that gap, as they allow for determinations in the low-q^2 region, although they suffer from systematic uncertainties that are challenging to evaluate.

We present in the following predictions the full set of local form factors. Instead, one can introduce a reduced set of form factors (soft form factors) in the heavy quark limit within the large recoil region. Under this approximation, only two independent form factors remain for $B \to K^*$ and only one for $B \to K$ [40]. This significantly reduces the uncertainties related to the form factors. Nonetheless, considering the correlations among the full form factors, a similar cancellation of the uncertainties can be obtained.

3.1. Lattice QCD

3.1.1. $B \to K$

The latest lattice results for the hadronic $B \to K$ form factors are given in [41] for the FNAL/MILC collaboration, and in [42] for the HPQCD collaboration. The FNAL/MILC results are obtained directly for the range $q^2 \geq 17$ GeV^2, and expanded to the whole q^2 range using the Boyd, Grinstein, and Lebed (BGL) parameterisation [43]. The total errors, which encompass both the statistical and the systematic uncertainties, are below 4% at high q^2. For lower q^2, the errors are of the order of 10% for f_+ and around 30% for f_T.

The recent determination by HPQCD [42] supersedes their previous results [44] and covers the entire q^2 range, sending the lattice spacing $a \to 0$ and simultaneously fitting them

using the Bourreley–Caprini–Lellouch (BCL) parameterisation [45]. This determination is highly precise, with quoted errors of less than 4% for f_+ and f_0 and less than 7% for f_T. Their results at $q^2 = 0\,\text{GeV}^2$ read as follows:

$$f_+(q^2 = 0) = f_0(q^2 = 0) = 0.332 \pm 0.012, \tag{40}$$

$$f_T(q^2 = 0, \mu = 4.8\,\text{GeV}) = 0.332 \pm 0.024. \tag{41}$$

Confirmation of this new determination using the new approach is still awaited from other lattice collaborations.

The Flavour Lattice Averaging Group [46] performed an average of the results from [41] and [44], which has not yet been updated to incorporate the latest HPQCD results.

3.1.2. $B \to K^*$

Lattice QCD results for the $B \to K^*$ local form factors are given in [47] and updated in [48]. These results are obtained directly at low recoil and extrapolated using their parameterisation. At $q^2 = 0\,\text{GeV}^2$, the results read as follows:

$$\begin{aligned} V(q^2 = 0) &= 0.31 \pm 0.15, & A_0(q^2 = 0) &= 0.351 \pm 0.074, \\ A_1(q^2 = 0) &= 0.303 \pm 0.051, & A_{12}(q^2 = 0) &= 0.251 \pm 0.053, \\ T_1(q^2 = 0) &= 0.291 \pm 0.044, & T_2(q^2 = 0) &= 0.291 \pm 0.044, \\ T_3(q^2 = 0) &= 0.50 \pm 0.10. \end{aligned} \tag{42}$$

The total error can reach up to $\mathcal{O}(50\%)$ at $q^2 = 0\,\text{GeV}^2$ due to the extrapolation, but it remains below 10% in the low-recoil region.

3.2. LCSR

LCSRs for hadronic transition form factors are derived from a vacuum-to-hadron correlation function, with two intermediate quark currents. In given kinematical conditions, this correlation function can be expanded through an operator product expansion near the light-cone (LCOPE), in terms of the hadron Light-Cone Distribution Amplitudes (LCDAs). For $B \to K^{(*)}$ transitions, the hadron can be either the light meson (here $K^{(*)}$) [49–54] or the B-meson [18,55–62]. The other hadron is then interpolated between the two quark currents which allows for the extraction of the form factor of interest. The light-meson LCDAs are generally known with a better accuracy, and higher-order corrections have been included. The use of B-meson LCDAs is more recent and carries larger uncertainties. There have been discrepant predictions for the B-meson LCDAs [63–67] with significant implications as demonstrated in [60], with an increase of up to 50% in $A_2^{B\to K^*}$ at $q^2 = 0\,\text{GeV}^2$. Nonetheless, they allow for a direct computation of a large set of form factors for different processes. Using B-meson LCDAs makes it possible to take into account in addition the effects of the finite width of the K^*-meson.

LCSRs rely on the semi-global quark–hadron duality [68], which induces a systematic error that is difficult to quantify. In [60], a regime of the LCSR method was introduced to mitigate this error; however, conclusive results for these form factors are still awaited.

3.2.1. $B \to K$

In [51], the form factors are obtained directly for $q^2 \leq 14\,\text{GeV}^2$ before extrapolating to the entire physical range. The results in [54] are expected to supersede those of [51], due to updates in inputs and the inclusion of higher-order corrections. In [54], results are directly derived for $q^2 < 12\,\text{GeV}^2$ and extrapolated to the entire physical range using the BCL parameterisation [45]. The LCSR results were later fitted in [20] by adding lattice points and using the parameterisation given in [53].

The results in [58] are computed for $q^2 \leq 5\,\text{GeV}^2$ and are then fitted with the z-expansion [53], including additional points from the lattice determination [44] to constrain

the high-q^2 region. The inclusion of lattice data does change the central values presented in Table 1. In a subsequent work [20], the authors advise against using their previous results [58] for $B \to K$ due to issues with the determination of the sum rule thresholds that are not yet understood. The authors of [57] work in the Soft-Collinear Effective Theory (SCET) framework, in which they computed the next-order QCD corrections that have not been included in [58]. However, they do not necessarily supersede the results of [58] where the framework is the Heavy Quark Effective Theory (HQET) and not SCET. Their results are obtained directly for $q^2 \leq q^2_{\text{cut}}$ where q^2_{cut} varies between 8 GeV^2 and 10 GeV^2. The extrapolation is performed using the BCL parameterisation [45], including the lattice results of [41,42].

Table 1. LCSR predictions for $B \to K$ form factors at $q^2 = 0$, where $f_0(q^2 = 0) = f_+(q^2 = 0)$.

Form Factor	Value at $q^2 = 0$	Ref.
f_+	$0.331 \pm 0.041 \pm \delta_{f_+}$ †	[51] *
	0.395 ± 0.033	[54] *
	0.27 ± 0.08	[58] **
	0.325 ± 0.085	[57] **
f_T	$0.358 \pm 0.037 \pm \delta_{f_T}$ †	[51] *
	0.351 ± 0.027	[54] *
	0.25 ± 0.07	[58] **
	0.351 ± 0.097	[57] **

†: $\delta_{f_{+,T}}$ accounts for the uncertainty in the first Gegenbauer moment. *: using K-meson LCDAs. **: using B-meson LCDAs.

3.2.2. $B \to K^*$

In [50], the form factors are obtained directly for $q^2 \leq 14$ GeV^2 before being extrapolated to the whole physical range. These results are superseded in [53] due to the updated inputs. They are also determined directly for q^2 below 14 GeV^2 and fitted using their modified z-expansion (BSZ). The numerical values presented in Table 2 are the result of the fit using only their LCSR results. Additional results for a fit adding lattice points from [48] are also presented, which slightly shift the values presented in Table 2.

Table 2. LCSR predictions for $B \to K^*$ form factors at $q^2 = 0$ where $T_2(q^2 = 0) = T_1(q^2 = 0)$. The linear combinations A_{12} and T_{23} are introduced in Appendix A.

Form Factor	Value at $q^2 = 0$	Ref.
A_1	$0.282 \pm 0.028 \pm \delta_{A_1}$ †	[50] *
	0.27 ± 0.03	[53] *
	$0.25^{+0.16}_{-0.10}$	[18] **
	0.26 ± 0.08	[58] **
A_2	$0.259 \pm 0.027 \pm \delta_{A_2}$ †	[50] *
	$0.23^{+0.19}_{-0.10}$	[18]**
	0.24 ± 0.09	[58] **
A_{12}	0.26 ± 0.03	[53] *
V	$0.411 \pm 0.033 \pm \delta_V$ †	[50] *
	0.34 ± 0.04	[53] *
	$0.36^{+0.23}_{-0.12}$	[18] **
	0.33 ± 0.11	[58] **
T_1	$0.333 \pm 0.028 \pm \delta_{T_1}$ †	[50] *
	0.28 ± 0.03	[53] *
	$0.31^{+0.18}_{-0.10}$	[18] **
	0.29 ± 0.10	[58] **
T_3	$0.202 \pm 0.018 \pm \delta_{T_3}$ †	[50] *
	$0.22^{+0.17}_{-0.10}$	[18] **
T_{23}	0.67 ± 0.08	[53] *
	0.58 ± 0.13	[58] **

†: δ_X accounts for the uncertainty in the first Gegenbauer moment. *: using K^*-meson LCDAs. **: using B-meson LCDAs.

In [18], the form factors are obtained at $q^2 < 12$ GeV^2 and are then fitted using the BCL-parameterisation [45]. These results are superseded in [58] due to the updated inputs and the inclusion of higher order in the LCOPE. They are computed for $q^2 \leq 5$ GeV^2 and are then fitted with the BSZ z-expansion [53], including additional points from the lattice determination [47,48] to constrain the high-q^2 region. The inclusion of lattice data does change the central values presented in Table 2.

An advantage of LCSRs with B-meson LCDAs is the possibility of computing form factors for decays such as $B \to K\pi$, where the final state is a dimeson state, which allows us to study of the impact of the finite width of the K^*-meson. This computation has been carried out in [61] for the P-wave $K\pi$ system, and then updated in [62] to add the contribution of the S-wave $K\pi$. In [61], a correction to the $B \to K^*$ form factors (using B-meson LCDAs) was obtained as a multiplicative factor of $\mathcal{W}_{K^*} \sim 1.1$. It corresponds to an enhancement in the decay rate $B \to K^*(\to K\pi)\ell\ell$ of $\mathcal{O}(20\%)$ but has a negligible impact on $P_5'(B \to K^*(\to K\pi)\ell\ell)$. In [62], the additional S-wave corrections are claimed to be small. This $\mathcal{W}_{K^*} \sim 1.1$ correction is valid only in the low-q^2 region, where it has been computed, and when using LCSR with B-meson LCDAs.

Since form factors are real analytic functions in the q^2 complex plane, up to a branch cut and a pole at the resonance, it is customary to use parameterisations respecting these constraints, such as the Caprini, Lellouch, and Neubert (CLN) parameterisation [69]; the Boyd, Grinstein, and Lebed (BGL) parameterisation [43]; the Bourrely, Caprini, and Lellouch (BCL) parameterisation [45]; the Bharucha, Straub, and Zwicky (BSZ) parametrisation [53]; and the Gubernari, van Dyk, and Virto (GvDV) parameterisation [19]. These parameterisations are used to extrapolate the results obtained for a limited range to the entire physical q^2 range. The z-expansions are in practice truncated and only the first terms are considered for the fits, which induces a systematic truncation error. Dispersive (or unitarity) bounds allow for the control of said truncation errors for a given parameterisation and have been used for B-meson decays [19,20,43,70–73].

The latest dispersive bound results for local $B \to K^{(*)}$ form factors have been obtained in [73] to which we refer for more details.

4. Non-Local Contributions

The long-distance effects in the $B \to K^{(*)}\ell\ell$ decays generated by four-quark and chromomagnetic dipole operators, sometimes referred to as charm-loop effects, are technically more challenging to derive than the local contributions. These long-distance effects were traditionally accounted for in the QCD factorisation framework and in the heavy quark limit for $q^2 < 7$ GeV^2. This calculation included up to weak annihilation, some non-factorisable contributions, and the hard spectator scattering [74,75]. However, in [20], it is suggested that this approach is reliable only below 4 GeV^2 and may overlook potentially significant power corrections. Even outside of the resonance region, intermediate and/or virtual $c\bar{c}$ states still contribute. An agnostic approach to take into account the effect of the power corrections is to consider a q^2- and transversity-dependent polynomial whose relative size is guesstimated [76].

Two approaches have emerged in recent years to take into account these effects in a more comprehensive manner, which we refer to in the following as the z-expansion [20] and the hadronic dispersion relation [77–81]. Both approaches start from a dispersion relation; however, they differ in their evaluation methods. The z-expansion approach evaluates the dispersion relation using an LCOPE at negative q^2 before extrapolating it to the physical range. In contrast, the hadronic dispersion relation is evaluated directly at the hadronic level within the physical range.

4.1. The z-Expansion

In the sum over accessible quark flavours in Equation (9), $\mathcal{H}_{u,\mu}^{B\to K^{(*)}}$ and $\mathcal{H}_{d,\mu}^{B\to K^{(*)}}$ are usually neglected as they are suppressed by CKM subleading matrix elements and/or small Wilson coefficients. The necessary formulas for $\mathcal{H}_{s,\mu}^{B\to K^{(*)}}$ and $\mathcal{H}_{b,\mu}^{B\to K^{(*)}}$ have been

derived in [74,75,82] in the QCD factorisation framework and in the heavy quark mass limit, and are given in Appendix C of [20].

The most significant and challenging contributions of $\mathcal{H}_{c,\mu}^{B\to K^{(*)}}$, however, have been treated differently. In the z-expansion approach [20], the non-local contributions $\mathcal{H}_{c,\mu}^{B\to K^{(*)}}$ are computed at negative values of q^2 using an LCOPE. At $q^2 = m_{J/\psi}^2$ these contributions are obtained from data on branching ratios and angular observables. This non-local form factor is then fitted via a z-expansion over the region $0 < q^2 < m_{J/\psi}^2$.

The LCOPE computation was performed in [19] considering only the dominant contributions from $\mathcal{O}_1^c$ and $\mathcal{O}_2^c$. In [20], contributions from penguin operators were added, but not from $\mathcal{O}_8$ as its contribution is considered negligible in this stage. The LCOPE expansion reads as follows:

$$\mathcal{H}_{c,\lambda}^{B\to K^{(*)}} = -\frac{1}{16\pi^2}\left(\frac{q^2}{2m_B^2}\Delta C_9 \mathcal{F}_\lambda^{B\to K^{(*)}} + \frac{m_b}{m_B}\Delta C_7 \mathcal{F}_{T,\lambda}^{B\to K^{(*)}}\right) + 2Q_c\left(C_2 - \frac{C_1}{2N_c}\right)\tilde{\mathcal{V}}_\lambda^{B\to K^{(*)}} + \text{higher-power corrections}, \tag{43}$$

where the basis of local form factors $\mathcal{F}_{(T),\lambda}^{B\to K^{(*)}}$ is introduced in Appendix C, the matching coefficients $\Delta C_{7,9}$ correspond to the leading power of non-local contributions, and $\tilde{\mathcal{V}}_\lambda^{B\to K^{(*)}}$ denotes subleading contributions that are not proportional to the local form factors. The matching coefficients $\Delta C_{7,9}$ have been computed to NLO in QCD [4,82–86] and are sometimes incorporated into the effective Wilson coefficients $C_{7,9}^{\text{eff}}$ which then become q^2-dependent. The term $\tilde{\mathcal{V}}_\lambda^{B\to K^{(*)}}$ was initially found to be sizeable in [18], but this computation has been superseded by that in [19] where it was determined to be negligible due to a more complete calculation which included the missing three-particle distribution amplitudes and updated the necessary inputs. Thus, in [20], to account for $\tilde{\mathcal{V}}_\lambda^{B\to K^{(*)}}$, only the uncertainty of the non-local form factors was increased.

The LCOPE results and the residue extracted from the data at $q^2 = m_{J/\psi}^2$ are then fitted with the z parameterisation described in [19]. The result is data-driven but can also be used with only the LCOPE results for extrapolation, although this leads to larger uncertainties.

Dispersive bounds for the non-local contributions were first derived in [20]. Imposing this dispersive bound for the long-distance effects significantly reduces the uncertainties. This dispersive bound can be further saturated by considering additional channels such as $\Lambda_b \to \Lambda\mu^+\mu^-$. The final results agree with the QCD factorisation approach; however, they exhibit larger uncertainties for the z-expansion method, especially near the J/ψ pole, which is not accounted for in QCD factorisation. Assuming that the z-expansion accounts for the whole amplitude, a careful assessment of the uncertainties is required to include all contributions.

4.2. The Hadronic Dispersion Relation

The evaluation of the long-distance effect in [80] for $B \to K\ell\ell$ and its subsequent extension in [81] to $B \to K^{(*)}\ell\ell$ follows a slightly different and predominantly data-driven approach. This strategy can be viewed as an extension of the procedures suggested in [77–79]. For $B \to K\mu\mu$ [80], the long-distance effects are incorporated into the effective Wilson coefficient:

$$C_9^{\text{eff}} = C_9 + Y_{c\bar{c}}(q^2) + Y_{\text{light}}(q^2) + Y_{\tau\bar{\tau}}(q^2), \tag{44}$$

where $Y_i(q^2)$ stands for the long-distance effect caused by the intermediate state i. Specifically, $Y_{c\bar{c}}$ accounts for the dominant contributions from $\mathcal{O}_1^c$ and $\mathcal{O}_2^c$ only, Y_{light} corresponds to the contributions from the subleading operators $\mathcal{O}_{3-6,8}$ and of $\mathcal{O}_{1-2}^u$, and $Y_{\tau\bar{\tau}}$ corresponds to the tau loop. Instead of using an LCOPE to evaluate the dispersion relations at negative q^2, as performed in [18–20], the dispersion relations here are evaluated directly at the hadronic level for positive q^2. For $Y_{c\bar{c}}$, single-particle intermediate states (J/ψ, $\psi(2S)$,

etc.) and two-particle states ($D\bar{D}$, $D^*\bar{D}$, etc.) are considered. For Y_{light}, given the loop or CKM suppression and the inclusion of intermediate states with charm valence quarks in $Y_{c\bar{c}}$, only vector single-particle states with light valence quarks (ρ, ω, ϕ) are taken into account. The hadronic contributions for single-particle intermediate states are modelled using Breit–Wigner distributions, while a more complex approximation is used for two-particle intermediate states. The relevant amplitude and phase parameters are extracted from experimental measurements. The dispersion relation for $Y_{c\bar{c}}$ is subtracted at $q^2 = 0$ to ensure convergence of the two-particle term, with the term at $q^2 = 0$ evaluated in QCD factorisation. The tau loop contribution is fully computed in perturbation theory.

For $B \to K^* \ell\ell$ [81], the correction to C_7 is treated as a universal shift estimated using perturbation theory [74]. The corrections $Y(q^2)$ to C_9 were evaluated as

$$Y^\lambda(q^2) = Y^\lambda_{c\bar{c}}(q^2) + Y^{[0]}_{q\bar{q}}(q^2) + Y^{[0]}_{b\bar{b}}(q^2)\,, \tag{45}$$

where λ denotes the polarisation. The charm-loop contribution $Y^\lambda_{c\bar{c}}$ was evaluated hadronically, similar to the approach in [80], while the other contributions were taken from perturbation theory at the lowest order in α_s. For explicit expressions, we refer the reader to [80].

The hadronic dispersion relation method has been implemented by LHCb in [87–89], revealing a persistent tension between Standard Model predictions and measurements. Overall, there is a strong agreement between the z-expansion and hadronic dispersion relation approaches. For visual comparisons, we refer the reader to the plots in [89].

In [90], the impact of the rescattering of intermediate hadronic states is discussed. These contributions are particularly challenging to estimate. Based on a data-driven analysis, it is argued in [90] that these contributions can potentially resolve the tension between SM predictions and experimental measurements, although a consensus has not yet been reached. In [91], an estimate of the rescattering of charmed and charmed-strange mesons has been performed for the $B^0 \to K^0 \ell\ell$ decay, which finds at most a 10% shift to C_9, insufficient to resolve the tension.

5. Other Sources of Uncertainties

In this section, we discuss the impact of QED corrections on the Wilson coefficients and the influence of CKM matrix elements on predictions and their discrepancies with experimental measurements. These effects are often overlooked but are becoming increasingly relevant given the current precision of both measurements and predictions.

5.1. Wilson Coefficients

The Wilson coefficients are calculated in perturbative theory and have been computed to NNLO in QCD [15,92,93]:

$$C_i(\mu) = C_i^{(0)} + \frac{\alpha_s(\mu)}{4\pi} C_i^{(1)} + \left(\frac{\alpha_s(\mu)}{4\pi}\right)^2 C_i^{(2)} + \mathcal{O}(\alpha_s^3), \tag{46}$$

where $C_i^{(n)}$ is the nth order of the Wilson coefficient in the α_s expansion. These coefficients are initially calculated at the electroweak scale $\mu_0 \sim M_W$ using a two-loop level computation, followed by the resummation of large logarithms and the evolution to the relevant scale $\mu_b \sim m_b$ using the three-loop Anomalous Dimension Matrix to account for operator mixing. Due to this operator mixing, it is customary to introduce the effective Wilson coefficients through the following combinations:

$$C_7^{\text{eff}}(\mu) = C_7(\mu) - \frac{1}{3}C_3(\mu) - \frac{4}{9}C_4(\mu) - \frac{20}{3}C_5(\mu) - \frac{80}{9}C_6(\mu), \tag{47}$$

$$C_8^{\text{eff}}(\mu) = C_8(\mu) + C_3(\mu) - \frac{1}{6}C_4(\mu) + 20C_5(\mu) - \frac{10}{3}C_6(\mu). \tag{48}$$

We emphasise that the notation C_7^{eff} used here arises solely from renormalisation and should not be confused with the use of effective Wilson coefficients in the context of non-local contributions, where "effective" refers to the inclusion of these non-local contributions within the Wilson coefficients.

QED corrections can also be computed and have been accounted for in [94,95]. Introducing the variable $\kappa(\mu) = \frac{\alpha(\mu)}{\alpha_s(\mu)}$, the perturbative expansion in both QED and QCD can be written as

$$C_i(\mu) = \sum_{n,m=0}^{2} \alpha_s(\mu)^n \kappa(\mu)^m C_i^{(n,m)}(\mu) + \mathcal{O}(\alpha_s^3, \kappa^3). \tag{49}$$

Numerical values of the Wilson coefficients including NNLO QCD and NLO QED (we note that for C_9 and C_{10}, the QED corrections are said to be at NNLO in [95], but the definition of the operators $\mathcal{O}_9$ and $\mathcal{O}_{10}$ is different from the one used here) corrections at the scale $\mu_b = 5$ GeV are reported in Table 3.

Table 3. Wilson coefficients at the scale $\mu_b = 5.0$ GeV. We use $\sin^2\theta_W = 0.231160$.

Wilson Coefficient	Value (QCD)	Correction (QED)
$C_1(\mu_b)$	-0.2477	-0.0030
$C_2(\mu_b)$	1.0080	0.0056
$C_3(\mu_b)$	-0.0049	-0.0000
$C_4(\mu_b)$	-0.0763	-0.0003
$C_5(\mu_b)$	0.0003	0.0000
$C_6(\mu_b)$	0.0009	0.0000
$C_7(\mu_b)$	-0.3180	0.0037
$C_8(\mu_b)$	-0.1710	0.0000
$C_9(\mu_b)$	4.1764	-0.1305
$C_{10}(\mu_b)$	-4.1494	-0.1445

The QED contributions induce small corrections to the Wilson coefficients, up to $\sim$3.5% for $C_{9,10}$ which are often neglected. Nevertheless, given the current precision, their inclusion is becoming increasingly relevant.

5.2. CKM

The determination of the CKM factor $\lambda_t = V_{tb}V_{ts}^*$ is particularly relevant for branching fractions, where the predictions scale with $|V_{tb}V_{ts}^*|^2$.

We use values from the Particle Data Group [96] where the Wolfenstein parameter fit was performed with over-constraining measurements (and for which unitarity of the CKM matrix is implied):

$$\begin{aligned} \lambda &= 0.22500 \pm 0.00067, & A &= 0.826^{+0.018}_{-0.015}, \\ \bar{\rho} &= 0.159 \pm 0.010, & \bar{\eta} &= 0.348 \pm 0.010, \end{aligned} \tag{50}$$

which sets the following values:

$$|V_{ts}| = 0.04110^{+0.00083}_{-0.00072}, |V_{tb}| = 0.999118^{+0.000031}_{-0.000036}. \tag{51}$$

Very similar results were obtained in the *CKM*fitter 2023 update [97] and the UTfit 2023 update [98], with differences in the CKM factor λ_t being well under a percent.

While the uncertainties in the CKM matrix elements are relatively small compared to the uncertainty on local and non-local form factors, and only amount to $\mathcal{O}(2\%)$ for $|V_{ts}|$, they can still have a significant impact on the predictions due to the dependence on $|V_{tb}V_{ts}^*|^2$. Between 2021 and 2022, the prediction of the $B \to K^{(*)}\mu\mu$ branching fraction has been shifted by $\mathcal{O}(5\%)$ due to the update of the CKM values. Moreover, if we reconsider the assumptions of BSM physics or unitarity, the CKM matrix elements are not immune to

further shifts or changes. In addressing constraints in the presence of BSM physics, a fit with tree-level inputs alone led to shifts of $\mathcal{O}(5\%)$ and larger uncertainties in [96].

Therefore, given the precision of measurements and predictions, careful consideration of the CKM matrix elements and the assumptions under which they are obtained is crucial when discussing SM predictions. Notably, P_5' serves as an ideal probe for NP due to its independence from CKM matrix elements by construction.

6. Impact on Predictions

We discuss in this section the impact of local form-factors and long-distance effects on the branching fraction $\mathcal{B}(B^+ \to K^+\mu\mu)$ and the angular observable $P_5'(B^0 \to K^{*0}\mu\mu)$ using the `SuperIso` public program [25,99–101]. For reference, we also plot the experimental results of LHCb [6] and CMS [7] for $\mathcal{B}(B^+ \to K^+\mu\mu)$ and LHCb [9] and CMS [13] for $P_5'(B^0 \to K^{*0}\mu\mu)$. The grey vertical bands starting at $q^2 = 6$ GeV^2 denote the region approaching the resonances, which is less reliable and sometimes disregarded. The error bars on the figures in this section represent the 1σ errors computed by considering the propagated uncertainties across all parameters and inputs.

6.1. Impact of Local Form Factors

As expected, the branching fraction $\mathcal{B}(B^+ \to K^+\mu\mu)$ is significantly influenced by the local form factors. The predictions shown in Figure 1a, based on form factors from [42], agree within the error bars with those from [54]. However, the observed tension with the measurements clearly depends on the specific set of form factors employed. Using the form factors from [42], for instance, reveals a reduced tension. In both cases, non-local contributions are adopted from [20].

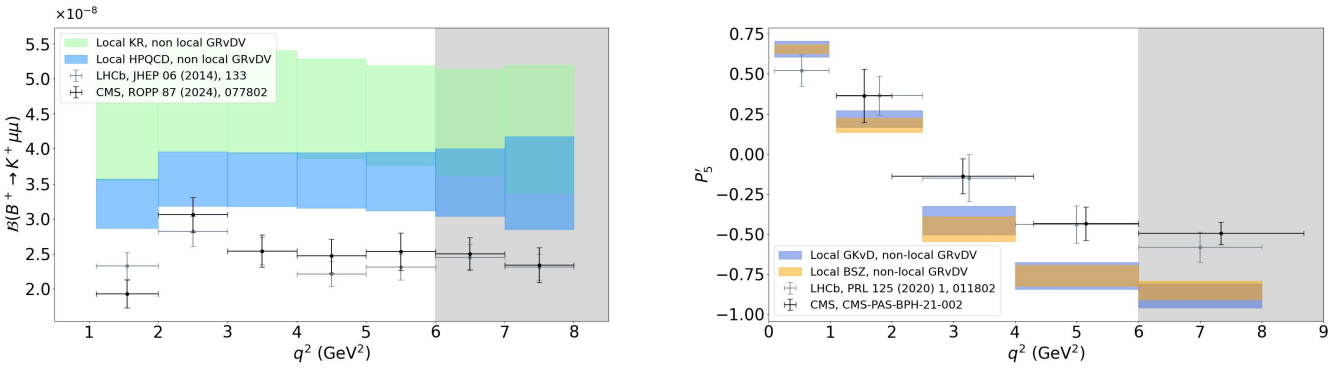

(**a**) (**b**)

Figure 1. Impact of local form factors on the prediction of (**a**) $\mathcal{B}(B^+ \to K^+\mu\mu)$ with local form factors from [54] (KR) and from [42] (HPQCD); (**b**) $P_5'(B_0 \to K^{*0}\mu\mu)$ with local form factors from [58] (GKvD) and from [53] (BSZ). For both, non-local form factors from [20], denoted as GRvDV, have been used.

The optimised angular observables such as P_5' are by construction less dependent on the local form factors, which is confirmed by the relatively small uncertainty on the predictions in Figure 1b. Moreover the different determinations of the local form factors [53,58] are in agreement and consistent in their tension with the experimental data.

6.2. Impact of Non-Local Form Factors

We compare the impact of non-local form factors obtained in QCD factorisation (QCDf) [74,75] with those determined using the more recent z-expansion approach [20]. The differences in central values for the branching fraction (Figure 2a) and the angular observable P_5' (Figure 2b) are small in both implementations. However, since the QCDf approach does not account for charm resonances, there is a noticeable difference in uncertainties for the branching fraction. Consequently, in the implementation of long-distance

effects in `SuperIso`, an error budget was guesstimated to account for the yet unknown power corrections when using QCDf results (see [76,102–107] for more details).

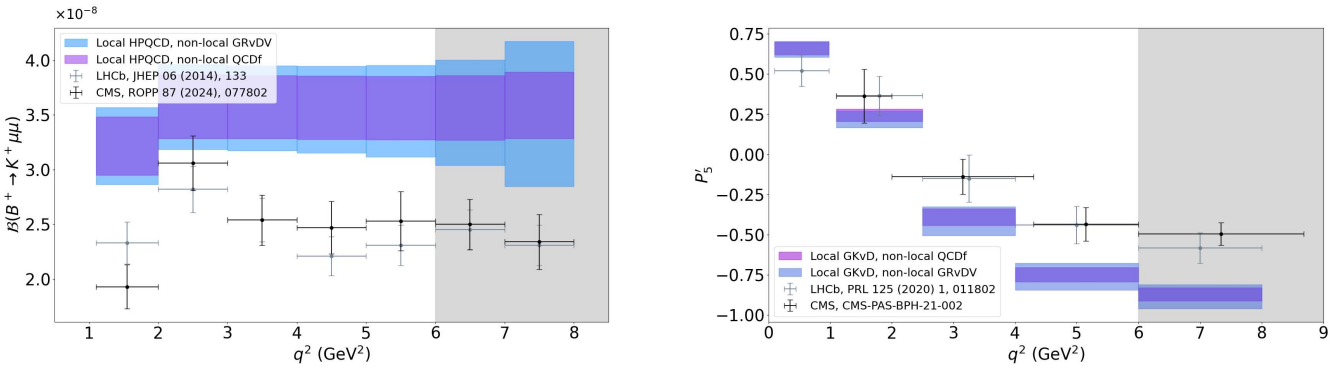

(**a**) (**b**)

Figure 2. Impact of non-local form factors on the prediction of (**a**) $\mathcal{B}(B^+ \to K^+\mu\mu)$ with local form factors from [42] (HQPCD), and non-local form factors from [74,75] (QCDf) and from [20] (GRvDV); (**b**) $P_5'(B_0 \to K^{*0}\mu\mu)$ with local form factors from [58] (GKvD), and non-local form factors from [74,75] (QCDf) and from [20] (GRvDV).

6.3. Impact of QED Corrections to Wilson Coefficients

We compare the impact of QED corrections to Wilson coefficients. These corrections are relatively minor and the resulting shift observed in the branching fraction $\mathcal{B}(B^+ \to K^+\mu\mu)$ in Figure 3a is negligible. However, their impact is more visible in P_5' as shown in Figure 3b, where they tend to reduce the tension between predictions and measurements.

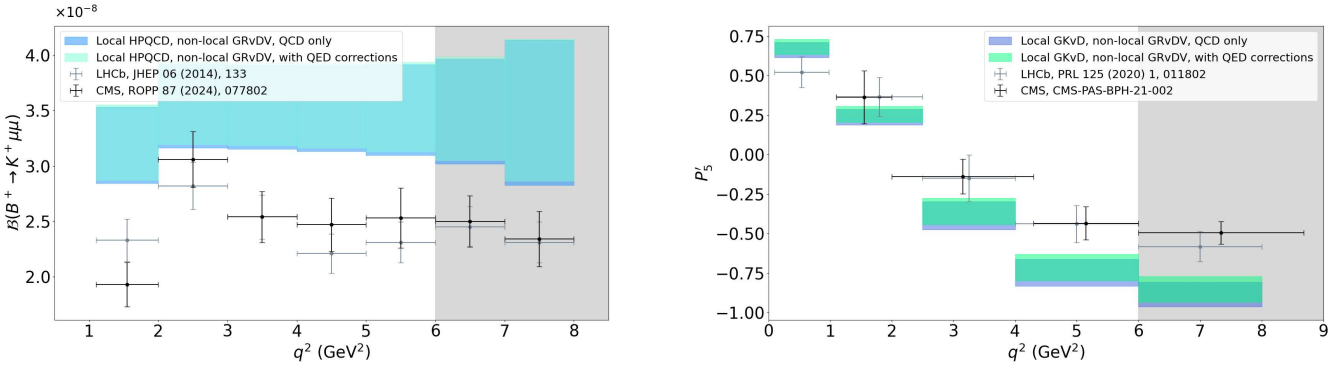

(**a**) (**b**)

Figure 3. Impact of QED corrections to Wilson coefficients on the prediction of (**a**) $\mathcal{B}(B^+ \to K^+\mu\mu)$ with local form factors from [42] (HPQCD) and non-local form factors from [20] (GRvDV); (**b**) $P_5'(B_0 \to K^{*0}\mu\mu)$ with local form factors from [58] (GKvD) and non-local form factors from [20] (GRvDV).

6.4. Impact of CKM Matrix Elements

We compare below the impact of the CKM matrix elements obtained from the fits in [96]: One with the full data, and one taking only into account tree-level inputs (Figure 4). There is a clear effect from the set of CKM parameters used when discussing the tension with the experimental data.

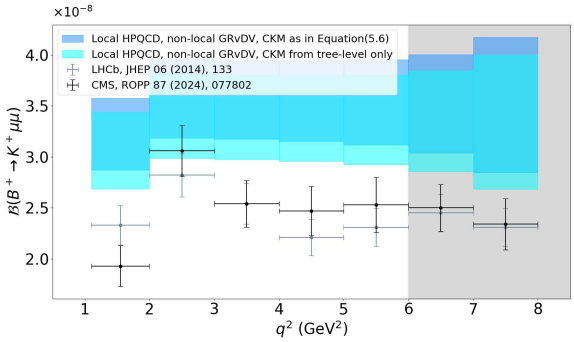

Figure 4. Impact of the CKM factor on the prediction of $\mathcal{B}(B^+ \to K^+\mu\mu)$ with local form factors from [42] (HPQCD) and non-local form factors from [20] (GRvDV).

7. Conclusions

Hints of NP beyond the SM in semi-leptonic B decays, particularly in the branching fraction $\mathcal{B}(B \to K\mu\mu)$ and the angular observable $P_5'(B \to K^*\mu\mu)$ at low q^2, still persist. However, unlike the $R_{K^{(*)}}$ ratios, accurately assessing the level of tension with experimental measurements for these observables is significantly more challenging. In this review, we addressed the theoretical calculations of $B \to K^{(*)}\ell\ell$ and the main sources of uncertainties.

The primary elements contributing to the remaining uncertainty in $B \to K^{(*)}\ell\ell$ decays are the local transition form factors and the long-distance contributions. Significant progress has been achieved in lattice QCD, particularly by the HPQCD collaboration, which has provided direct results for $f_{+,T}^{B\to K}$ across the entire q^2 range. Nevertheless, as we await similar results for $B \to K^*$, and a cross-check for $B \to K$, LCSRs remain relevant. Despite all predictions for the relevant form factors being consistent within their uncertainties, they significantly influence the predictions, with the tension reduced when using the HPQCD form factor set. Optimised angular observables such as P_5' are less sensitive to local form factors, and furthermore, the discrepancies among various determinations of local $B \to K^*$ form factors are smaller. However, it is crucial to note that LCSRs with B-meson LCDAs heavily rely on B-LCDA parameters, which currently exhibit discrepancies and can lead to substantial variations in the local form factors at $q^2 = 0\,\text{GeV}^2$, up to $\mathcal{O}(50\%)$.

Both types of observables are impacted by the non-local effects, although different estimates of these effects are in agreement. While the QCD factorisation framework initially provided an estimate of these non-local effects, more recent methods have emerged such as the z-expansion, which computes charm-loop contributions using an LCOPE at negative q^2, and the hadronic dispersion relation, evaluated predominantly at the hadronic level within the physical range, and have yielded consistent results. It is worth noting that, in this stage, the different evaluations of the non-local contributions do not resolve the discrepancies between theoretical predictions and experimental results; nonetheless, it is not excluded that some contributions (e.g., the rescattering of intermediate hadronic states) with potentially significant effects have been overlooked.

Finally, we discussed the impact of QED corrections on the Wilson coefficients. While their effect on branching fractions is negligible, this is less the case for angular observables. Furthermore, careful consideration is warranted regarding the CKM matrix elements, given that the assumptions used to determine them have a substantial impact on branching fractions and other observables that are sensitive to them.

In recent years, there have been remarkable improvements in the predictions of $B \to K^{(*)}\ell\ell$, and we expect this progress to continue, leading to increasingly precise predictions, and further constraints or hints on New Physics signatures.

Author Contributions: Conceptualization, F.M.; writing—original draft preparation, Y.M.; writing—review and editing, Y.M., F.M.; supervision, F.M. All authors have read and agreed to the published version of the manuscript.

Funding: This research was funded in part by the National Research Agency (ANR) under project ANR-21-CE31-0002-01.

Data Availability Statement: The data supporting the conclusions of this article will be made available by the authors on request.

Acknowledgments: The authors are grateful to A. Carvunis, S. Neshatpour, and T. Hurth for useful discussions.

Conflicts of Interest: The authors declare no conflict of interest.

Appendix A. Definition of Local Hadronic form Factors

A suitable form factor basis for the $B \to K$ transition is $f_0^{B\to K}$, $f_+^{B\to K}$, and $f_T^{B\to K}$, which are defined as

$$\begin{aligned}\langle K(k)|\bar{q}_1\gamma^\mu b|B(p_B)\rangle &= \left[(p_B+k)^\mu - \frac{m_B^2-m_P^2}{q^2}q^\mu\right]f_+^{B\to K} + \frac{m_B^2-m_P^2}{q^2}q^\mu f_0^{B\to K},\\ \langle K(k)|\bar{q}_1\sigma^{\mu\nu}q_\nu b|B(p_B)\rangle &= \frac{if_T^{B\to K}}{m_B+m_P}\Big[q^2(p_B+k)^\mu - \Big(m_B^2-m_P^2\Big)q^\mu\Big].\end{aligned} \tag{A1}$$

For $\bar{B} \to \bar{K}^*$, we used the form factors $V^{B\to K^*}$, $A_0^{B\to K^*}$, $A_1^{B\to K^*}$, $A_2^{B\to K^*}$, $T_1^{B\to K^*}$, $T_2^{B\to K^*}$, and $T_3^{B\to K^*}$, which can be defined as

$$\begin{aligned}\langle K^*(k,\eta)|\bar{q}_1\gamma^\mu b|B(p_B)\rangle =&\epsilon^{\mu\nu\rho\sigma}\eta_\nu^* p_{B\rho}k_\sigma\frac{2V^{B\to K^*}}{m_B+m_{K^*}},\\ \langle K^*(k,\eta)|\bar{q}_1\gamma^\mu\gamma_5 b|B(p_B)\rangle =&i\eta_\nu^*\Bigg[q^\mu q^\nu\frac{2m_{K^*}}{q^2}A_0^{B\to K^*} + \left(g^{\mu\nu}-\frac{q^\mu q^\nu}{q^2}\right)(m_B+m_{K^*})A_1^{B\to K^*}\\ &-\left(\frac{(p_B+k)^\mu q^\nu}{m_B+m_{K^*}} - \frac{q^\mu q^\nu}{q^2}(m_B-m_{K^*})\right)A_2^{B\to K^*}\Bigg],\\ \langle K^*(k,\eta)|\bar{q}_1 i\sigma^{\mu\nu}q_\nu b|B(p_B)\rangle =&-\epsilon^{\mu\nu\rho\sigma}\eta_\nu^* p_{B\rho}k_\sigma 2T_1^{B\to K^*},\\ \langle K^*(k,\eta)|\bar{q}_1 i\sigma^{\mu\nu}q_\nu\gamma_5 b|B(p_B)\rangle =&i\eta_\nu^*\Big[\Big(g^{\mu\nu}\Big(m_B^2-m_{K^*}^2\Big)-(p_B+k)^\mu q^\nu\Big)T_2^{B\to K^*}\\ &+q^\nu\left(q^\mu-\frac{q^2}{m_B^2-m_{K^*}^2}(p_B+k)^\mu\right)T_3^{B\to K^*}\Big],\end{aligned} \tag{A2}$$

The variables p_B, k, and q represent the momenta of the B-meson, the $K^{(*)}$-meson, and the momentum transfer, respectively. η denotes the polarisation of the K^*-meson. We adopt the convention $\epsilon_{0123} = +1$.

It is convenient to introduce the following linear combination of form factors A_{12} and T_{23} as

$$A_{12} \equiv \frac{(m_B+m_{K^*})^2(m_B^2-m_{K^*}^2-q^2)A_1 - \lambda(m_B^2,m_{K^*}^2,q^2)A_2}{16m_B m_{K^*}^2(m_B+m_{K^*})}, \tag{A3}$$

$$T_{23} \equiv \frac{(m_B^2-m_{K^*}^2)(m_B^2+3m_{K^*}^2-q^2)T_2 - \lambda(m_B^2,m_{K^*}^2,q^2)T_3}{8m_B m_{K^*}^2(m_B-m_{K^*})}. \tag{A4}$$

Appendix B. Angular Conventions

We collect below more precise definitions of the angles relevant to the $\bar{B} \to \bar{K}^*\ell\ell$ decay. Let us define the symmetric and antisymmetric momenta:

$$\begin{aligned}\overrightarrow{P}^i_{\ell^-\ell^+} &= \overrightarrow{p_{\ell^-}} + \overrightarrow{p_{\ell^+}}, & \overrightarrow{Q}^i_{\ell^-\ell^+} &= \overrightarrow{p_{\ell^-}} - \overrightarrow{p_{\ell^+}},\\ \overrightarrow{P}^i_{K\pi} &= \overrightarrow{p_K} + \overrightarrow{p_\pi}, & \overrightarrow{Q}^i_{K\pi} &= \overrightarrow{p_K} - \overrightarrow{p_\pi},\end{aligned} \tag{A5}$$

where the superscript i indicates in which particle's rest frame the momenta are evaluated.

The angles defined with the convention in Section 2.2 can then be expressed as

$$\begin{aligned}
\cos\theta_\ell &= \frac{\overrightarrow{Q}^{\ell\ell}_{\ell^-\ell^+}\cdot\overrightarrow{P}^{\ell\ell}_{K\pi}}{|\overrightarrow{Q}^{\ell\ell}_{\ell^-\ell^+}||\overrightarrow{P}^{\ell\ell}_{K\pi}|}, & \cos\phi &= \frac{(\overrightarrow{Q}^{\bar{B}}_{\ell^-\ell^+}\times\overrightarrow{P}^{\bar{B}}_{\ell^-\ell^+})}{|\overrightarrow{Q}^{\bar{B}}_{\ell^-\ell^+}||\overrightarrow{P}^{\bar{B}}_{\ell^-\ell^+}|}\cdot\frac{(\overrightarrow{Q}^{\bar{B}}_{K\pi}\times\overrightarrow{P}^{\bar{B}}_{K\pi})}{|\overrightarrow{Q}^{\bar{B}}_{K\pi}||\overrightarrow{P}^{\bar{B}}_{K\pi}|},\\
\cos\theta_K &= -\frac{\overrightarrow{Q}^{K^*}_{K\pi}\cdot\overrightarrow{P}^{K^*}_{\ell^-\ell^+}}{|\overrightarrow{Q}^{K^*}_{K\pi}||\overrightarrow{P}^{K^*}_{\ell^-\ell^+}|}, & \sin\phi &= \left(\frac{(\overrightarrow{Q}^{\bar{B}}_{\ell^-\ell^+}\times\overrightarrow{P}^{\bar{B}}_{\ell^-\ell^+})}{|\overrightarrow{Q}^{\bar{B}}_{\ell^-\ell^+}||\overrightarrow{P}^{\bar{B}}_{\ell^-\ell^+}|}\times\frac{(\overrightarrow{Q}^{\bar{B}}_{K\pi}\times\overrightarrow{P}^{\bar{B}}_{K\pi})}{|\overrightarrow{Q}^{\bar{B}}_{K\pi}||\overrightarrow{P}^{\bar{B}}_{K\pi}|}\right)\cdot\frac{\overrightarrow{P}^{\bar{B}}_{K\pi}}{|\overrightarrow{P}^{\bar{B}}_{K\pi}|}.
\end{aligned} \tag{A6}$$

We refer to [34] for a detailed discussion on the different conventions, both theoretical and the ones used by LHCb, and how to convert between them.

Appendix C. Alternate Basis

We relate the usual form factor basis that we use to the one presented in [20], as well as the equivalence between the F_i functions for $B\to K\ell\ell$ and the transversity amplitudes for $\bar{B}\to\bar{K}^*\ell\ell$ with the transversity amplitudes in [20].

Appendix C.1. $B\to K$

The transversity amplitudes introduced in [20] for the $B\to K\ell\ell$ transition read as follows:

$$\mathcal{A}^{K\ell\ell}_{\lambda,L(R)} = \mathcal{N}^{K\ell\ell}\left\{(C_9\mp C_{10})\mathcal{F}^{B\to K}_\lambda + \frac{2m_bm_B}{q^2}\left[C_7\mathcal{F}^{B\to K}_{T,\lambda} - 16\pi^2\frac{m_B}{m_b}\mathcal{H}^{B\to K}_\lambda\right]\right\}, \tag{A7}$$

where $\mathcal{N}^{K\ell\ell} = \sqrt{\lambda(m_B^2,m_K^2,q^2)\times\mathcal{C}(q^2)}$ and $\lambda = 0$, t refers to the longitudinal or timelike polarisation, respectively, with $\mathcal{F}^{B\to K}_{T,t} = \mathcal{H}^{B\to K}_t = 0$. The form factor basis in [20] is related to the one we use and introduced in Appendix A by

$$\begin{aligned}
\mathcal{F}_0 &= f_+^{B\to P},\\
\mathcal{F}_t &= f_0^{B\to P},
\end{aligned}\qquad \mathcal{F}_{T,0} = \frac{q^2}{m_B(m_B+m_K)}f_T^{B\to P}. \tag{A8}$$

The F_i functions introduced in Section 2.1 are related to the transversity amplitudes (A7) as:

$$\begin{aligned}
F_V(q^2) &= \frac{1}{\mathcal{N}^{K\ell\ell}}\frac{\mathcal{A}_{0,L}+\mathcal{A}_{0,R}}{2}, & F_A(q^2) &= \frac{1}{\mathcal{N}^{K\ell\ell}}\frac{\mathcal{A}_{0,R}-\mathcal{A}_{0,L}}{2},\\
F_P(q^2) &= -\frac{m_\ell}{\mathcal{N}^{K\ell\ell}}\left(\frac{\mathcal{A}_{0,R}-\mathcal{A}_{0,L}}{2} + \frac{m_B^2-m_K^2}{q^2}\left(\frac{\mathcal{A}_{t,L}-\mathcal{A}_{t,R}}{2}+\frac{\mathcal{A}_{0,R}-\mathcal{A}_{0,L}}{2}\right)\right),
\end{aligned} \tag{A9}$$

and

$$\delta F_V = -\frac{32\pi^2m_B^2}{q^2}\mathcal{H}_0^{B\to K}. \tag{A10}$$

Appendix C.2. $B\to K^*$

The transversity amplitudes introduced in [58] for the $B\to K^*\ell\ell$ transition read as follows:

$$\mathcal{A}^{K^*\ell\ell}_{\lambda,L(R)} = \mathcal{N}^{K^*\ell\ell}\left\{(C_9\mp C_{10})\mathcal{F}^{B\to K^*}_\lambda + \frac{2m_bm_B}{q^2}\left[C_7\mathcal{F}^{B\to K^*}_{T,\lambda} - 16\pi^2\frac{m_B}{m_b}\mathcal{H}^{B\to K^*}_\lambda\right]\right\}, \tag{A11}$$

where $\mathcal{N}^{K^*\ell\ell} = N\times m_B$ and $\lambda = \perp, \parallel, 0, t$ refers to the different polarisations, with $\mathcal{F}^{B\to K^*}_{T,t} = \mathcal{H}^{B\to K^*}_t = 0$. We further introduce $\mathcal{A}^{K^*\ell\ell}_t = \mathcal{A}^{K^*\ell\ell}_{t,L} - \mathcal{A}^{K^*\ell\ell}_{t,R}$. Their form factor basis is related to the one we use and introduced in Appendix A by

$$\mathcal{F}_\perp = \frac{\sqrt{2\,\lambda(m_B^2, m_{K^*}^2, q^2)}}{m_B(m_B + m_{K^*})} V, \qquad \mathcal{F}_\parallel = \frac{\sqrt{2}(m_B + m_{K^*})}{m_B} A_1,$$
$$\mathcal{F}_0 = \frac{(m_B^2 - m_{K^*}^2 - q^2)(m_B + m_{K^*})^2 A_1 - \lambda(m_B^2, m_{K^*}^2, q^2) A_2}{2m_{K^*} m_B^2 (m_B + m_{K^*})},$$
$$\mathcal{F}_t = A_0, \quad \mathcal{F}_{T,\perp} = \frac{\sqrt{2\,\lambda(m_B^2, m_{K^*}^2, q^2)}}{m_B^2} T_1, \quad \mathcal{F}_{T,\parallel} = \frac{\sqrt{2}(m_B^2 - m_{K^*}^2)}{m_B^2} T_2,$$
$$\mathcal{F}_{T,0} = \frac{q^2(m_B^2 + 3m_{K^*}^2 - q^2)}{2m_B^3 m_{K^*}} T_2 - \frac{q^2 \lambda(m_B^2, m_{K^*}^2, q^2)}{2m_B^3 m_{K^*}(m_B^2 - m_{K^*}^2)} T_3. \tag{A12}$$

The transversity amplitudes $A^{K^*\ell\ell}_{\lambda,L(R)}$ introduced in Section 2.2 are related to the transversity amplitudes $\mathcal{A}^{K^*\ell\ell}_{\lambda,L(R)}$ by

$$A^{K^*\ell\ell}_{\perp,L(R)} = \mathcal{A}^{K^*\ell\ell}_{\perp,L(R)}, \qquad A^{K^*\ell\ell}_{\parallel,L(R)} = -\mathcal{A}^{K^*\ell\ell}_{\parallel,L(R)},$$
$$A^{K^*\ell\ell}_{0,L(R)} = -\frac{m_B}{\sqrt{q^2}} \mathcal{A}^{K^*\ell\ell}_{0,L(R)}, \qquad A^{K^*\ell\ell}_{t} = -\frac{1}{m_B}\sqrt{\frac{\lambda(m_B^2, m_{K^*}^2, q^2)}{q^2}}\, \mathcal{A}^{K^*\ell\ell}_{t}. \tag{A13}$$

Similarly,

$$\delta A^{K^*\ell\ell}_{\perp,L(R)} = -32\pi^2 N \frac{m_B^3}{q^2} \mathcal{H}^{K^*\ell\ell}_{\perp,L(R)}, \qquad \delta A^{K^*\ell\ell}_{\parallel,L(R)} = +32\pi^2 N \frac{m_B^3}{q^2} \mathcal{H}^{K^*\ell\ell}_{\parallel,L(R)},$$
$$\delta A^{K^*\ell\ell}_{0,L(R)} = +32\pi^2 N \frac{m_B^4}{q^2\sqrt{q^2}} \mathcal{H}^{K^*\ell\ell}_{0,L(R)}. \tag{A14}$$

References

1. Chatrchyan, S.; Khachatryan, V.; Sirunyan, A.M.; Tumasyan, A.; Adam, W.; Aguilo, E.; Bergauer, T.; Dragicevic, M.; Erö, J.; Fabjan, C.; et al. Observation of a New Boson at a Mass of 125 GeV with the CMS Experiment at the LHC. *Phys. Lett. B* **2012**, *716*, 30–61. [CrossRef]
2. Aad, G.; Abajyan, T.; Abbott, B.; Abdallah, J.; Khalek, S.A.; Abdelalim, A.; Abdinov, O.; Aben, R.; Abi, B.; Abolins, M.; et al. Observation of a new particle in the search for the Standard Model Higgs boson with the ATLAS detector at the LHC. *Phys. Lett. B* **2012**, *716*, 1–29. [CrossRef]
3. Aaij, R.; Abdelmotteleb, A.S.W.; Beteta, C.A.; Abudinén, F.; Ackernley, T.; Adeva, B.; Adinolfi, M.; Adlarson, P.; Afsharnia, H.; Agapopoulou, C.; et al. Measurement of lepton universality parameters in $B^+ \to K^+\ell^+\ell^-$ and $B^0 \to K^{*0}\ell^+\ell^-$ decays. *Phys. Rev. D* **2023**, *108*, 032002. [CrossRef]
4. Bell, G.; Huber, T. Master integrals for the two-loop penguin contribution in non-leptonic B-decays. *J. High Energy Phys.* **2014**, *12*, 129. [CrossRef]
5. Lees, J.P.; Poireau, V.; Tisserand, V.; Tico, J.G.; Grauges, E.; Palano, A.; Eigen, G.; Stugu, B.; Brown, D.N.; Kerth, L.T.; et al. Measurement of Branching Fractions and Rate Asymmetries in the Rare Decays $B \to K^{(*)}l^+l^-$. *Phys. Rev. D* **2012**, *86*, 032012. [CrossRef]
6. Aaij, R.; The LHCb collaboration; Adeva, B.; Adinolfi, M.; Affolder, A.; Ajaltouni, Z.; Albrecht, J.; Alessio, F.; Alexander, M.; Ali, S.; et al. Differential branching fractions and isospin asymmetries of $B \to K^{(*)}\mu^+\mu^-$ decays. *J. High Energy Phys.* **2014**, *06*, 133. [CrossRef]
7. CMS Collaboration. Test of lepton flavor universality in and decays in proton-proton collisions at. *Rept. Prog. Phys.* **2024**, *87*, 077802. [CrossRef] [PubMed]
8. Aaij, R.; Beteta, C.A.; Ackernley, T.; Adeva, B.; Adinolfi, M.; Afsharnia, H.; Aidala, C.A.; Aiola, S.; Ajaltouni, Z.; Akar, S.; et al. Angular Analysis of the $B^+ \to K^{*+}\mu^+\mu^-$ Decay. *Phys. Rev. Lett.* **2021**, *126*, 161802. [CrossRef]
9. Aaij, R.; Beteta, C.A.; Ackernley, T.; Adeva, B.; Adinolfi, M.; Afsharnia, H.; Aidala, C.A.; Aiola, S.; Ajaltouni, Z.; Akar, S.; et al. Measurement of *CP*-Averaged Observables in the $B^0 \to K^{*0}\mu^+\mu^-$ Decay. *Phys. Rev. Lett.* **2020**, *125*, 011802. [CrossRef]
10. Sirunyan, A.M.; Tumasyan, A.; Adam, W.; Ambrogi, F.; Asilar, E.; Bergauer, T.; Brandstetter, J.; Brondolin, E.; Dragicevic, M.; Erö, J.; et al. Measurement of angular parameters from the decay $B^0 \to K^{*0}\mu^+\mu^-$ in proton-proton collisions at $\sqrt{s} = 8$ TeV. *Phys. Lett. B* **2018**, *781*, 517–541. [CrossRef]

11. Wehle, S.; Niebuhr, C.; Yashchenko, S.; Adachi, I.; Aihara, H.; Al Said, S.; Asner, D.M.; Aulchenko, V.; Aushev, T.; Ayad, R.; et al. Lepton-Flavor-Dependent Angular Analysis of $B \to K^* \ell^+ \ell^-$. *Phys. Rev. Lett.* **2017**, *118*, 111801. [CrossRef] [PubMed]
12. Aaboud, M.; Aad, G.; Abbott, B.; Abdinov, O.; Abeloos, B.; Abid i, S.H.; AbouZeid, O.S.; Abraham, N.L.; Abramowicz, H.; Abreu, H.;et al. Angular analysis of $B_d^0 \to K^* \mu^+ \mu^-$ decays in pp collisions at $\sqrt{s} = 8$ TeV with the ATLAS detector. *J. High Energy Phys.* **2018**, *10*, 47. [CrossRef]
13. CMS Collaboration. *Angular Analysis of the* $B^0 \to K^{*0}(892)\mu^+\mu^-$ *Decay at* $\sqrt{s}$ *= 13 TeV*; Technical Report; CERN: Geneva, Switzerland, 2024.
14. Buchalla, G.; Buras, A.J.; Lautenbacher, M.E. Weak decays beyond leading logarithms. *Rev. Mod. Phys.* **1996**, *68*, 1125–1144. [CrossRef]
15. Bobeth, C.; Misiak, M.; Urban, J. Photonic penguins at two loops and m_t dependence of $BR[B \to X_s l^+ l^-]$. *Nucl. Phys. B* **2000**, *574*, 291–330. [CrossRef]
16. Bobeth, C.; Buras, A.J.; Kruger, F.; Urban, J. QCD corrections to $\bar{B} \to X_{d,s} \nu \bar{\nu}$, $\bar{B}_{d,s} \to \ell^+ \ell^-$, $K \to \pi \nu \bar{\nu}$ and $K_L \to \mu^+ \mu^-$ in the MSSM. *Nucl. Phys. B* **2002**, *630*, 87–131. [CrossRef]
17. Chetyrkin, K.G.; Misiak, M.; Munz, M. $|\Delta F| = 1$ nonleptonic effective Hamiltonian in a simpler scheme. *Nucl. Phys. B* **1998**, *520*, 279–297. [CrossRef]
18. Khodjamirian, A.; Mannel, T.; Pivovarov, A.A.; Wang, Y.M. Charm-loop effect in $B \to K^{(*)} \ell^+ \ell^-$ and $B \to K^* \gamma$. *J. High Energy Phys.* **2010**, *9*, 89. [CrossRef]
19. Gubernari, N.; van Dyk, D.; Virto, J. Non-local matrix elements in $B_{(s)} \to \{K^{(*)}, \phi\} \ell^+ \ell^-$. *J. High Energy Phys.* **2021**, *2*, 88. [CrossRef]
20. Gubernari, N.; Reboud, M.; van Dyk, D.; Virto, J. Improved theory predictions and global analysis of exclusive $b \to s \mu^+ \mu^-$ processes. *J. High Energy Phys.* **2022**, *9*, 133. [CrossRef]
21. Isidori, G.; Nabeebaccus, S.; Zwicky, R. QED corrections in $\bar{B} \to \bar{K} \ell^+ \ell^-$ at the double-differential level. *J. High Energy Phys.* **2020**, *12*, 104. [CrossRef]
22. Isidori, G.; Lancierini, D.; Nabeebaccus, S.; Zwicky, R. QED in $\bar{B} \to \bar{K} \ell^+ \ell^-$ LFU ratios: Theory versus experiment, a Monte Carlo study. *J. High Energy Phys.* **2022**, *10*, 146. [CrossRef]
23. Choudhury, D.; Das, D.; Das, J. Soft photon corrections in $B \to K^{(*)} \ell^+ \ell^-$ and $\Lambda_b \to \Lambda^{(*)} \ell^+ \ell^-$ decays. *arXiv* **2023**, arXiv:2307.07578. Available online: http://arxiv.org/abs/2307.07578 (accessed on 1 July 2024).
24. Golonka, P.; Was, Z. PHOTOS Monte Carlo: A Precision tool for QED corrections in Z and W decays. *Eur. Phys. J. C* **2006**, *45*, 97–107. [CrossRef]
25. Mahmoudi, F. SuperIso v2.3: A Program for calculating flavor physics observables in Supersymmetry. *Comput. Phys. Commun.* **2009**, *180*, 1579–1613. [CrossRef]
26. Becirevic, D.; Kosnik, N.; Mescia, F.; Schneider, E. Complementarity of the constraints on New Physics from $B_s \to \mu^+ \mu^-$ and from $B \to K l^+ l^-$ decays. *Phys. Rev. D* **2012**, *86*, 034034. [CrossRef]
27. Bobeth, C.; Hiller, G.; Piranishvili, G. Angular distributions of $\bar{B} \to \bar{K} \ell^+ \ell^-$ decays. *J. High Energy Phys.* **2007**, *12*, 40. [CrossRef]
28. Kim, C.S.; Kim, Y.G.; Lu, C.D.; Morozumi, T. Azimuthal angle distribution in $B \to K * (\to K\pi) l^+ l^-$ at low invariant $m(l^+ l^-)$ region. *Phys. Rev. D* **2000**, *62*, 034013. [CrossRef]
29. Altmannshofer, W.; Ball, P.; Bharucha, A.; Buras, A.J.; Straub, D.M.; Wick, M. Symmetries and Asymmetries of $B \to K^* \mu^+ \mu^-$ Decays in the Standard Model and Beyond. *J. High Energy Phys.* **2009**, *1*, 19. [CrossRef]
30. Kruger, F.; Sehgal, L.M.; Sinha, N.; Sinha, R. Angular distribution and CP asymmetries in the decays $\bar{B} \to K^- \pi^+ e^- e^+$ and $\bar{B} \to \pi^- \pi^+ e^- e^+$. *Phys. Rev. D* **2000**, *61*, 114028. [CrossRef]
31. Egede, U.; Hurth, T.; Matias, J.; Ramon, M.; Reece, W. New observables in the decay mode $\bar{B}_d \to \bar{K}^{*0} l^+ l^-$. *J. High Energy Phys.* **2008**, *11*, 32. [CrossRef]
32. Bobeth, C.; Hiller, G.; Piranishvili, G. CP Asymmetries in bar $B \to \bar{K}^* (\to \bar{K}\pi) \bar{\ell}\ell$ and Untagged $\bar{B}_s$, $B_s \to \phi (\to K^+ K^-) \bar{\ell}\ell$ Decays at NLO. *J. High Energy Phys.* **2008**, *7*, 106. [CrossRef]
33. Egede, U.; Hurth, T.; Matias, J.; Ramon, M.; Reece, W. New physics reach of the decay mode $\bar{B} \to \bar{K}^{*0} \ell^+ \ell^-$. *J. High Energy Phys.* **2010**, *10*, 56. [CrossRef]
34. Gratrex, J.; Hopfer, M.; Zwicky, R. Generalised helicity formalism, higher moments and the $B \to K_{J_K} (\to K\pi) \bar{\ell}_1 \ell_2$ angular distributions. *Phys. Rev. D* **2016**, *93*, 054008. [CrossRef]
35. Matias, J.; Mescia, F.; Ramon, M.; Virto, J. Complete Anatomy of $\bar{B}_d \to \bar{K}^{*0} (\to K\pi) l^+ l^-$ and its angular distribution. *J. High Energy Phys.* **2012**, *4*, 104. [CrossRef]
36. Beaujean, F.; Bobeth, C.; van Dyk, D.; Wacker, C. Bayesian Fit of Exclusive $b \to s \bar{\ell}\ell$ Decays: The Standard Model Operator Basis. *J. High Energy Phys.* **2012**, *8*, 30. [CrossRef]
37. Feldmann, T.; Matias, J. Forward backward and isospin asymmetry for $B \to K^* l^+ l^-$ decay in the standard model and in supersymmetry. *J. High Energy Phys.* **2003**, *1*, 74. [CrossRef]
38. Bobeth, C.; Hiller, G.; van Dyk, D. The Benefits of $\bar{B} \to \bar{K}^* l^+ l^-$ Decays at Low Recoil. *J. High Energy Phys.* **2010**, *7*, 98. [CrossRef]
39. Descotes-Genon, S.; Matias, J.; Ramon, M.; Virto, J. Implications from clean observables for the binned analysis of $B \to K^* \mu^+ \mu^-$ at large recoil. *J. High Energy Phys.* **2013**, *1*, 48. [CrossRef]
40. Beneke, M.; Feldmann, T. Symmetry breaking corrections to heavy to light B meson form-factors at large recoil. *Nucl. Phys. B* **2001**, *592*, 3–34. [CrossRef]

41. Bailey, J.A.; Bazavov, A.; Bernard, C.; Bouchard, C.M.; DeTar, C.; Du, D.; El-Khadra, A.X.; Foley, J.; Freeland, E.D.; Gámiz, E.; et al. $B \to Kl^+l^-$ Decay Form Factors from Three-Flavor Lattice QCD. *Phys. Rev. D* **2016**, *93*, 025026. [CrossRef]
42. Parrott, W.G.; Bouchard, C.; Davies, C.T.H. B→K and D→K form factors from fully relativistic lattice QCD. *Phys. Rev. D* **2023**, *107*, 014510. [CrossRef]
43. Boyd, C.G.; Grinstein, B.; Lebed, R.F. Constraints on form-factors for exclusive semileptonic heavy to light meson decays. *Phys. Rev. Lett.* **1995**, *74*, 4603–4606. [CrossRef] [PubMed]
44. Bouchard, C.; Lepage, G.P.; Monahan, C.; Na, H.; Shigemitsu, J. Rare decay $B \to K\ell^+\ell^-$ form factors from lattice QCD. *Phys. Rev. D* **2013**, *88*, 054509; Erratum in *Phys. Rev. D* **2013**, *88*, 079901. [CrossRef]
45. Bourrely, C.; Caprini, I.; Lellouch, L. Model-independent description of B → pi l nu decays and a determination of |V(ub)|. *Phys. Rev. D* **2009**, *79*, 013008; Erratum in *Phys. Rev. D* **2010**, *82*, 099902. [CrossRef]
46. Aoki, Y.; Blum, T.; Colangelo, G.; Collins, S.; Della Morte, M.; Dimopoulos, P.; Dürr, S.; Feng, X.; Fukaya, H.; Golterman, M.; et al. FLAG Review 2021. *Eur. Phys. J. C* **2022**, *82*, 869. [CrossRef]
47. Horgan, R.R.; Liu, Z.; Meinel, S.; Wingate, M. Lattice QCD calculation of form factors describing the rare decays $B \to K^*\ell^+\ell^-$ and $B_s \to \phi\ell^+\ell^-$. *Phys. Rev. D* **2014**, *89*, 094501. [CrossRef]
48. Horgan, R.R.; Liu, Z.; Meinel, S.; Wingate, M. Rare *B* decays using lattice QCD form factors. *Proc. Sci.* **2015**, *214*, 372. [CrossRef]
49. Braun, V.M. QCD sum rules for heavy flavors. *Proc. Sci.* **1999**, *3*, 6, [CrossRef]
50. Ball, P.; Zwicky, R. $B_{d,s} \to \rho, \omega, K^*, \phi$ decay form-factors from light-cone sum rules revisited. *Phys. Rev. D* **2005**, *71*, 014029. [CrossRef]
51. Ball, P.; Zwicky, R. New results on $B \to \pi, K, \eta$ decay formfactors from light-cone sum rules. *Phys. Rev. D* **2005**, *71*, 014015. [CrossRef]
52. Duplancic, G.; Melic, B. B, B(s) → K form factors: An Update of light-cone sum rule results. *Phys. Rev. D* **2008**, *78*, 054015. [CrossRef]
53. Bharucha, A.; Straub, D.M.; Zwicky, R. $B \to V\ell^+\ell^-$ in the Standard Model from light-cone sum rules. *J. High Energy Phys.* **2016**, *8*, 98. [CrossRef]
54. Khodjamirian, A.; Rusov, A.V. $B_s \to K\ell\nu_\ell$ and $B_{(s)} \to \pi(K)\ell^+\ell^-$ decays at large recoil and CKM matrix elements. *J. High Energy Phys.* **2017**, *8*, 112. [CrossRef]
55. Khodjamirian, A.; Mannel, T.; Offen, N. Form-factors from light-cone sum rules with *B*-meson distribution amplitudes. *Phys. Rev. D* **2007**, *75*, 054013. [CrossRef]
56. Lü, C.D.; Shen, Y.L.; Wang, Y.M.; Wei, Y.B. QCD calculations of $B \to \pi, K$ form factors with higher-twist corrections. *J. High Energy Phys.* **2019**, *1*, 24. [CrossRef]
57. Cui, B.Y.; Huang, Y.K.; Shen, Y.L.; Wang, C.; Wang, Y.M. Precision calculations of $B_{d,s} \to \pi$, K decay form factors in soft-collinear effective theory. *J. High Energy Phys.* **2023**, *3*, 140. [CrossRef]
58. Gubernari, N.; Kokulu, A.; van Dyk, D. $B \to P$ and $B \to V$ Form Factors from *B*-Meson Light-Cone Sum Rules beyond Leading Twist. *J. High Energy Phys.* **2019**, *1*, 150. [CrossRef]
59. Monceaux, Y.; Carvunis, A.; Mahmoudi, F. LCSR predictions for $b \to s$ hadronic form factors. *Proc. Sci.* **2023**, *445*, 60. [CrossRef]
60. Carvunis, A.; Mahmoudi, F.; Monceaux, Y. On the potential of Light-Cone Sum Rules without Quark-Hadron Duality. *arXiv* **2024**, arXiv:2404.01290.
61. Descotes-Genon, S.; Khodjamirian, A.; Virto, J. Light-cone sum rules for $B \to K\pi$ form factors and applications to rare decays. *J. High Energy Phys.* **2019**, *12*, 83. [CrossRef]
62. Descotes-Genon, S.; Khodjamirian, A.; Virto, J.; Vos, K.K. Light-Cone Sum Rules for *S*-wave $B \to K\pi$ Form Factors. *J. High Energy Phys.* **2023**, *6*, 34. [CrossRef]
63. Wang, Y.M.; Shen, Y.L. QCD corrections to B → π form factors from light-cone sum rules. *Nucl. Phys. B* **2015**, *898*, 563–604. [CrossRef]
64. Braun, V.M.; Ivanov, D.Y.; Korchemsky, G.P. The B meson distribution amplitude in QCD. *Phys. Rev. D* **2004**, *69*, 034014. [CrossRef]
65. Khodjamirian, A.; Mandal, R.; Mannel, T. Inverse moment of the B_s-meson distribution amplitude from QCD sum rule. *J. High Energy Phys.* **2020**, *10*, 43. [CrossRef]
66. Nishikawa, T.; Tanaka, K. QCD Sum Rules for Quark-Gluon Three-Body Components in the B Meson. *Nucl. Phys. B* **2014**, *879*, 110–142. [CrossRef]
67. Rahimi, M.; Wald, M. QCD sum rules for parameters of the *B*-meson distribution amplitudes. *Phys. Rev. D* **2021**, *104*, 016027. [CrossRef]
68. Colangelo, P.; Khodjamirian, A. QCD sum rules, a modern perspective. In *At the Frontier of Particle Physics: Handbook of QCD*; Shifman, M., Ioffe, B., Eds.; World Scientific: Singapore, 2000; Volumes 1–3, pp. 1495–1576.
69. Caprini, I.; Lellouch, L.; Neubert, M. Dispersive bounds on the shape of anti-B → D(*) lepton anti-neutrino form-factors. *Nucl. Phys. B* **1998**, *530*, 153–181. [CrossRef]
70. De Rafael, E.; Taron, J. Constraints on heavy meson form-factors. *Phys. Lett. B* **1992**, *282*, 215–220. [CrossRef]
71. De Rafael, E.; Taron, J. Analyticity properties and unitarity constraints of heavy meson form-factors. *Phys. Rev. D* **1994**, *50*, 373–380. [CrossRef]

72. Boyd, C.G.; Grinstein, B.; Lebed, R.F. Model independent extraction of |V(cb)| using dispersion relations. *Phys. Lett. B* **1995**, *353*, 306–312. [CrossRef]
73. Gubernari, N.; Reboud, M.; van Dyk, D.; Virto, J. Dispersive analysis of B → K$^{(*)}$ and B$_s$→ ϕ form factors. *J. High Energy Phys.* **2023**, *12*, 153. [CrossRef]
74. Beneke, M.; Feldmann, T.; Seidel, D. Systematic approach to exclusive $B \to Vl^+l^-$, $V\gamma$ decays. *Nucl. Phys. B* **2001**, *612*, 25–58. [CrossRef]
75. Beneke, M.; Feldmann, T.; Seidel, D. Exclusive radiative and electroweak $b \to d$ and $b \to s$ penguin decays at NLO. *Eur. Phys. J. C* **2005**, *41*, 173–188. [CrossRef]
76. Hurth, T.; Mahmoudi, F. On the LHCb anomaly in $B \to K^*\ell^+\ell^-$. *J. High Energy Phys.* **2014**, *4*, 97. [CrossRef]
77. Lyon, J.; Zwicky, R. Resonances gone topsy turvy—The charm of QCD or new physics in $b \to s\ell^+\ell^-$? *arXiv* **2014**, arXiv:1406.0566. Available online: http://arxiv.org/abs/1406.0566 (accessed on 1 July 2024).
78. Braß, S.; Hiller, G.; Nisandzic, I. Zooming in on $B \to K^*\ell\ell$ decays at low recoil. *Eur. Phys. J. C* **2017**, *77*, 16. [CrossRef]
79. Blake, T.; Egede, U.; Owen, P.; Petridis, K.A.; Pomery, G. An empirical model to determine the hadronic resonance contributions to $\bar{B}^0 \to \bar{K}^{*0}\mu^+\mu^-$ transitions. *Eur. Phys. J. C* **2018**, *78*, 453. [CrossRef]
80. Cornella, C.; Isidori, G.; König, M.; Liechti, S.; Owen, P.; Serra, N. Hunting for $B^+ \to K^+\tau^+\tau^-$ imprints on the $B^+ \to K^+\mu^+\mu^-$ dimuon spectrum. *Eur. Phys. J. C* **2020**, *80*, 1095. [CrossRef]
81. Bordone, M.; isidori, G.; Mächler, S.; Tinari, A. Short- vs. long-distance physics in $B \to K^{(*)}\ell^+\ell^-$: A data-driven analysis. *arXiv* **2024**, arXiv:2401.18007. Available online: http://arxiv.org/abs/2401.18007 (accessed on 1 July 2024).
82. Asatrian, H.M.; Greub, C.; Virto, J. Exact NLO matching and analyticity in $b \to s\ell\ell$. *J. High Energy Phys.* **2020**, *4*, 12. [CrossRef]
83. Asatryan, H.H.; Asatrian, H.M.; Greub, C.; Walker, M. Calculation of two loop virtual corrections to $b \to sl^+l^-$ in the standard model. *Phys. Rev. D* **2002**, *65*, 074004. [CrossRef]
84. Greub, C.; Pilipp, V.; Schupbach, C. Analytic calculation of two-loop QCD corrections to $b \to sl^+l^-$ in the high q^2 region. *J. High Energy Phys.* **2008**, *12*, 40. [CrossRef]
85. Ghinculov, A.; Hurth, T.; Isidori, G.; Yao, Y.P. The Rare decay $B \to X_s l^+l^-$ to NNLL precision for arbitrary dilepton invariant mass. *Nucl. Phys. B* **2004**, *685*, 351–392. [CrossRef]
86. De Boer, S. Two loop virtual corrections to $b \to (d,s)\ell^+\ell^-$ and $c \to u\ell^+\ell^-$ for arbitrary momentum transfer. *Eur. Phys. J. C* **2017**, *77*, 801. [CrossRef]
87. Aaij, R.; LHCb Collaboration; Adeva, B.; Adinolfi, M.; Ajaltouni, Z.; Akar, S.; Albrecht, J.; Alessio, F.; Alexander, M.; Ali, S.; et al. Measurement of the phase difference between short- and long-distance amplitudes in the $B^+ \to K^+\mu^+\mu^-$ decay. *Eur. Phys. J. C* **2017**, *77*, 161. [CrossRef]
88. Aaij, R.; Abdelmotteleb, A.S.W.; Beteta, C.A.; Abudinén, F.; Ackernley, T.; Adeva, B.; Adinolfi, M.; Adlarson, P.; Agapopoulou, C.; Aidala, C.A.; et al. Determination of short- and long-distance contributions in $B^0 \to K^{*0}\mu^+\mu^-$ decays. *Phys. Rev. D* **2024**, *109*, 052009. [CrossRef]
89. Aaij, R.; Abdelmotteleb, A.S.W.; Beteta, C.A.; Abudinén, F.; Ackernley, T.; Adefisoye, A.A.; Adeva, B.; Adinolfi, M.; Adlarson, P.; Agapopoulou, C.; et al. Comprehensive analysis of local and nonlocal amplitudes in the $B^0 \to K^{*0}\mu^+\mu^-$ decay. *arXiv* **2024**, arXiv:2405.17347. Available online: http://arxiv.org/abs/2405.17347 (accessed on 1 July 2024).
90. Ciuchini, M.; Fedele, M.; Franco, E.; Paul, A.; Silvestrini, L.; Valli, M. Constraints on lepton universality violation from rare B decays. *Phys. Rev. D* **2023**, *107*, 055036. [CrossRef]
91. Isidori, G.; Polonsky, Z.; Tinari, A. An explicit estimate of charm rescattering in $B^0 \to K^0\bar{\ell}\ell$. *arXiv* **2024**, arXiv:2405.17551. Available online: http://arxiv.org/abs/2405.17551 (accessed on 1 July 2024).
92. Misiak, M.; Steinhauser, M. Three loop matching of the dipole operators for $b \to s\gamma$ and $b \to sg$. *Nucl. Phys. B* **2004**, *683*, 277–305. [CrossRef]
93. Gorbahn, M.; Haisch, U. Effective Hamiltonian for non-leptonic $|\Delta F| = 1$ decays at NNLO in QCD. *Nucl. Phys. B* **2005**, *713*, 291–332. [CrossRef]
94. Bobeth, C.; Gambino, P.; Gorbahn, M.; Haisch, U. Complete NNLO QCD analysis of $\bar{B} \to X(s)l^+l^-$ and higher order electroweak effects. *J. High Energy Phys.* **2004**, *4*, 71. [CrossRef]
95. Huber, T.; Lunghi, E.; Misiak, M.; Wyler, D. Electromagnetic logarithms in $\bar{B} \to X_s l^+l^-$. *Nucl. Phys. B* **2006**, *740*, 105–137. [CrossRef]
96. Particle Data Group; Workman, R.L.; Burkert, V.D.; Crede, V.; Klempt, E.; Thoma, U.; Tiator, L.; Agashe, K.; Aielli, G.; Allanach, B.C.; et al. Review of Particle Physics. *Prog. Theor. Exp. Phys.* **2022**, *2022*, 083C01. [CrossRef]
97. Vale Silva, L. 2023 update of the extraction of the CKM matrix elements. In Proceedings of the 12th International Workshop on the CKM Unitarity Triangle, Santiago de Compostela, Spain, 18–22 September 2023.
98. Bona, M.; Ciuchini, M.; Derkach, D.; Ferrari, F.; Franco, E.; Lubicz, V.; Martinelli, G.; Morgante, D.; Pierini, M.; Silvestrini, L.; et al. New UTfit Analysis of the Unitarity Triangle in the Cabibbo-Kobayashi-Maskawa scheme. *Rend. Lincei Sci. Fis. Nat.* **2023**, *34*, 37–57. [CrossRef]
99. Mahmoudi, F. SuperIso: A Program for calculating the isospin asymmetry of $B \to K^*\gamma$ in the MSSM. *Comput. Phys. Commun.* **2008**, *178*, 745–754. [CrossRef]
100. Neshatpour, S.; Mahmoudi, F. Flavour Physics with SuperIso. *Proc. Sci.* **2021**, *392*, 36. [CrossRef]
101. Neshatpour, S.; Mahmoudi, F. Flavour Physics Phenomenology with SuperIso. *Proc. Sci.* **2022**, *409*, 10. [CrossRef]

102. Hurth, T.; Mahmoudi, F.; Neshatpour, S. On the anomalies in the latest LHCb data. *Nucl. Phys. B* **2016**, *909*, 737–777. [CrossRef]
103. Chobanova, V.G.; Hurth, T.; Mahmoudi, F.; Martinez Santos, D.; Neshatpour, S. Large hadronic power corrections or new physics in the rare decay $B \to K^* \mu^+ \mu^-$?. *J. High Energy Phys.* **2017**, *7*, 25. [CrossRef]
104. Hurth, T.; Mahmoudi, F.; Martinez Santos, D.; Neshatpour, S. Lepton nonuniversality in exclusive $b \to s\ell\ell$ decays. *Phys. Rev. D* **2017**, *96*, 095034. [CrossRef]
105. Arbey, A.; Hurth, T.; Mahmoudi, F.; Neshatpour, S. Hadronic and New Physics Contributions to $b \to s$ Transitions. *Phys. Rev. D* **2018**, *98*, 095027. [CrossRef]
106. Hurth, T.; Mahmoudi, F.; Neshatpour, S. Implications of the new LHCb angular analysis of $B \to K^* \mu^+ \mu^-$: Hadronic effects or new physics? *Phys. Rev. D* **2020**, *102*, 055001. [CrossRef]
107. Hurth, T.; Mahmoudi, F.; Neshatpour, S. B anomalies in the post $R_{K^{(*)}}$ era. *Phys. Rev. D* **2023**, *108*, 115037. [CrossRef]